Cement and Concrete Research 173 (2023) 107283

Contents lists available at ScienceDirect

Cement and Concrete Research

journal homepage: www.elsevier.com/locate/cemconres

Alkali metal distribution in composite cement pastes and its relation to accelerated ASR tests

Petter Hemstad [a,*], Pamela Zuschlag [a], Petter Kjellemyr [a], Jan Lindgård [a,b], Knut O. Kjellsen [c], Terje F. Rønning [d], Harald Justnes [b], Maciej Zajac [e], Mohsen Ben Haha [e], Klaartje De Weerdt [a]

[a] Department of Structural Engineering, NTNU, Trondheim, Norway
[b] SINTEF Community, Trondheim, Norway
[c] Heidelberg Materials Sement Norge AS, Norway
[d] Heidelberg Materials Northern Europe, Norway
[e] Heidelberg Materials Global R&D, Germany

ARTICLE INFO

Keywords:
Pore solution
Cement paste
Alkali-aggregate reaction
Alkalis
pH
Temperature
Durability
Fly ash
Pozzolan
Expansion
Calcium-silicate-hydrate (C-S-H)
SEM
EDX
X-ray diffraction
Thermal analysis

ABSTRACT

Accelerated testing of alkali silica reaction (ASR) in concrete at elevated temperatures of 38 and 60 °C has an unknown impact on the alkali metal distribution in the cement paste. This paper investigates how the alkali metals released from hydrating Portland cement, limestone, and SCMs distribute between non-reactive and unreacted phases, C-A-S-H, and the pore solution. The SCMs investigated were fly ash and a volcanic pozzolan. The hydrate assemblage and pore solution of cement pastes cured at 20, 38 and 60 °C were analysed and related to the expansion of concrete prisms. There is little difference in alkali metal distribution at 20 and 38 °C, whereas curing at 60 °C has a large impact for the SCM containing blends. At alkali metal concentrations in the pore solution below 0.5 mol/L (Na + K) expansion of concrete was suppressed. Pore solution analysis could be used to screen new SCMs for ASR mitigation.

1. Introduction

The alkali-silica reaction (ASR) is one of the most widespread deterioration mechanisms in concrete, affecting structures across the world [1]. It occurs when the highly alkaline pore solution interacts with reactive silica in the aggregates, resulting in an expansive alkali silica gel. Depending on the reactivity of the aggregate, the chosen cement, and the environmental conditions, ASR typically acts on a scale from a few years up to several decades, though some extremely reactive aggregates can cause deterioration after a few months [2]. As the reaction proceeds, the concrete swells. This can result in reduction in service life, expensive repair, or total structural failure [3].

In concrete the alkali metals Na and K can originate from the aggregates [4] or external sources [5], though the main source is typically the cement. During the hydration of cement, Na and K are released into the pore solution by reacting phases such as alkali sulphates, clinker minerals and glassy phases in supplementary cementitious materials (SCM) [6,7]. As calcium-aluminium-silicate hydrate (C-A-S-H) precipitates, some of the alkali metal cations adsorb on its negatively charged surface [8–10]. In a mature cement paste the alkali metals are therefore distributed between non-reactive phases, unreacted phases, C-A-S-H, and the pore solution. Non-reactive refers to stable alkali metal bearing minerals that are unlikely to react, such as biotite and sanidine [11]. Unreacted on the other hand refers to phases that can react, but at a given time has not yet dissolved and released their alkali metals. In this work we use the term unreacted to refer to the sum of all these phases, including clinker minerals, other reactive minerals, and amorphous phases in SCMs.

The pore solution composition is crucial for ASR as it occurs via the pore solution through a dissolution/precipitation reaction. The alkali

* Corresponding author at: Richard Birkelands vei 1A, 7491 Trondheim, Norway.
E-mail address: petter.hemstad@ntnu.no (P. Hemstad).

https://doi.org/10.1016/j.cemconres.2023.107283
Received 15 May 2023; Received in revised form 5 July 2023; Accepted 19 July 2023
Available online 9 August 2023

metals in the pore solution are mostly present as monovalent cations (Na^+ and K^+) which are charge balanced by OH^- ions, giving rise to the typical high pH of cement pore solution (12.8–13.7). It is the pH of the pore solution which controls the dissolution of the silicate phases [12], where higher OH^- concentration and thereby higher pH leads to faster dissolution. A threshold for the OH^- concentration in the pore solution has been observed below which no considerable expansion occurs. The threshold ranges from 0.3 to 0.65 mol/L depending on the conditions of the accelerated expansion tests and the type of reactive aggregate used [7,13–18].

A common method to mitigate ASR is replacing part of the Portland cement (PC) with pozzolanic SCMs [19]. One of the main mechanisms by which these SCMs mitigate ASR is by reducing the alkali metal concentration in the pore solution, which in turn lowers the concentration of OH^- and the pH of the pore solution [19–22]. This is attributed to the pozzolanic reaction of the SCMs, as it provides silicate and aluminates to the solution which react with Portlandite (CH, $Ca(OH)_2$) to form C-A-S-H [23]. The C-A-S-H in these cements has a lower Ca/Si-ratio and higher Al/Si-ratio than in pure PC pastes [24,25], which improves its ability to bind alkali metal cations from the pore solution [8,10,20,26]. SCMs can also contribute with additional Al to the pore solution, which appears to slow down the dissolution of reactive silica [12,27].

ASR is a very slow reaction at ambient temperatures around 20 °C. Cases of expansion and damage in field can go undiagnosed for decades. Most data on ASR from laboratory studies comes from performance tests carried out at elevated temperatures of 38, 60, or 80 °C which accelerates the reaction. Concerns have however been raised as to the applicability of these tests [28–30]. One reason for this is that the reaction of included SCMs is also likely to be accelerated, which could lead to an overestimation of their mitigation efficiency. Another reason is the shifts in chemical equilibria that occurs at higher temperature, such as the destabilization of ettringite and subsequent increase in sulphate concentration [31]. The increase in sulphate has also been linked to increased dissolution rate of various silicate species [12]. Vollpracht et al. [32] reviewed the effect of SCMs on the pore solution of pastes cured at 20 °C. They highlighted the lack of published data regarding how curing temperature influences the pore solution composition in cement pastes containing SCMs.

SCMs such as natural pozzolans and fly ashes typically contain a considerable amount of alkali metals, in some cases even exceeding the alkali metal content of PC [33,34]. Despite this, even SCMs with high alkali content can be used to mitigate ASR. This raises the question about what portion of the alkalis in SCMs are available and can contribute to ASR [7,35]. Total Na_2O_{eq} is not a good measure of the alkali metal contribution of the SCM, as a portion of Na and K may be tied up in non-reactive crystalline phases [14]. The ASTM C311 test is used to determine the available alkali from a particular SCM. It exposes 5 g of pozzolan to 2 g of CH and 10 mL of water at 38 °C for 28 days, after which the hydrated mixture is ground and washed with hot water to leach the available alkali metals. The interpretation of the available alkali measured with this method is not straight forward as it reflects the alkali dissolved from the SCM minus those still bound in the hydration products after leaching [33]. Kalina et al. [11] characterized the crystalline phases in the SCMs and reported this in combination with the total and available alkali metal content, demonstrating that parts of the unavailable alkali metals are bound in non-reactive minerals. A way to build on this work would be to also estimate the share of alkali metals in the non-reactive minerals, consider the degree of reaction of the SCMs, evaluating the amount of C-A-S-H formed, and the amounts of alkali metal adsorbed on the C-A-S-H. To the authors knowledge no such studies have been published.

ASR regulations for concrete with reactive aggregates typically put an upper limit for the total alkali metal content in the concrete [36]. For plain PC concrete the limits are typically between 2.5 [37] and 3.5 Na_2O_{eq}/m^3 concrete [36,38,39]. In some recommendations the upper limit also depends on aggregate reactivity [38]. The total alkali content in the concrete is mainly governed by the alkali metal content in the cement (e.g., 0.6 wt% Na_2O_{eq}) and the amount of cement in the concrete (e.g., 450 kg/m^3 concrete). Alternatively, a specific total alkali content is documented for each specific composite cement which is typically higher than for a plain PC concrete (e.g. 6.5 kg Na_2O_{eq}/m^3 concrete for standard Norwegian fly ash cement). Such specific alkali limits are determination by using laboursome RILEM AAR-10 performance testing [40]. These regulations are all based on the total alkali metal content of the concrete mix, despite the fact that only the alkali metals in the pore solution contribute to ASR [19]. In some cases, the contribution of the alkali metals of the SCM is neglected or a lower proportion of these alkali metals are included in the calculation of the total alkali content in the concrete [38].

Because the pore solution controls ASR, several researchers have related the alkali metal concentration in the pore solution to expansion [7,12,15,41–45]. However, only a handful have expressed the alkali metal content present in the pore solution as a share of the total alkali content by multiplying concentrations with the pore solution volume [33,46,47]. Many also only report the concentrations of Na and K, whilst there are other elements in solution like Al and S that can also influence ASR [12]. Most studies of pore solutions focus on cement pastes cured at room temperature (20–23 °C), a good summary of these can be found in the review by Vollpracht et al. [32]. A limited number of studies have investigated the pore solution composition at the elevated temperatures used for expansion testing [15,16,47–51], but to our knowledge none have systematically compared the impact of increasing the temperature from 20 to 60 °C on the pore solution composition and linked it to ASR expansion.

Very few researchers have determined the uptake of alkali metals in the C-A-S-H and linked this to the pore solution composition and potential for ASR expansion [14,47]. When looking into cement hydration studies on composite cement, we find studies looking systematically into the effect of the curing temperature on the hydration products and pore solution [31,43,52], but not how this relates to ASR.

Alkali metal mass balances have been investigated by Rivard et al., but only for concrete without SCMs cured at 38 °C with the purpose to determine the share of alkali leached during accelerated expansion testing and the alkali taken up by aggregates and ASR products [46,53]. The only studies which, to the authors' knowledge, calculated an alkali metal distribution for cement paste containing SCMs are Taylor [54] and Duchesne and Bérubé [47]. They analysed the pore solution and determined the alkali adsorption by C-A-S-H, though in order to put up the balance they had to assume a degree of reaction for the PC and SCMs, the share of alkali in the SCMs available for ASR, the pore solution volume, and the hydrate assemblage. We wish to further refine their approach by experimentally determining these input parameters and putting up a full mass balance of the system. In addition, we include limestone as a non-pozzolanic filler to study PC dilution and systematically vary the curing temperature to understand the impact of SCMs on the risk of ASR expansion during accelerated testing.

Our goal with the present work is to link the total alkali metal content used by engineers to the alkali metal concentration in the pore solution, by providing a more fundamental understanding of the impact of the SCMs on the system. We develop a methodology to find the alkali metal distribution in cement pastes by quantifying the total Na and K content and determining how the alkali metals distribute after hydration. We use experiments and calculations to determine the amounts of Na and K present in unreacted and non-reactive phases, adsorbed on C-A-S-H, and free in the pore solution. The purpose of this approach is to focus on the fundamental chemical understanding of how SCMs influence ASR, rather than examining individual SCMs by trial and error.

To isolate the impact of the SCMs on the hydration products and pore solution, we simplify the system by focussing on sealed cured cement paste. We have therefore not considered the role of the aggregates on the alkali metal balance (both as a potential source and sink), nor the impact

of leaching or external alkali, even though these are known to play a considerable role in the alkali metal balance in concrete [29,46,53]. We have also limited the scope to one curing time of 180 days, although the time dependency between ASR and pore solutions is important [55].

The developed methodology enables us to understand how SCMs and elevated temperatures influence the alkali metal distribution between non-reactive phases, unreacted phases, pore solution, and C-A-S-H. There are three questions we seek to answer. Firstly, how are the alkali metals Na and K distributed in the hydrated cement paste? Secondly, how is the distribution of Na and K affected when PC is partially replaced by limestone or SCMs? Finally, how is the distribution of Na and K affected by elevating the curing temperature from 20 to 38 and 60 °C?

We do this by combining a detailed hydration study using experimental characterization of the hydrated cement paste, pore solution analysis, and a mass balance in order to put up a full alkali metal distribution, with ASR expansion measurements on concrete. We will be focusing on two SCMs, a traditional siliceous fly ash (FA) and a new source of volcanic pozzolan (VP). A total of four different hydrated cement pastes are investigated in depth: A reference cement with 100 % Portland cement (PC), a limestone reference with 22 % PC replaced with limestone (PC-L), and two cements with 18 % FA or VP with 4 % limestone (PC-FA and PC-VP). These are cured in sealed containers for 180 days at 20, 38, and 60 °C, before we analyse the solid phases and expressed pore solutions. The experimental results feed into a mass balance model to determine the hydrate assemblage, which is then used to calculate the alkali metal distribution in the investigated systems. Concurrently, concrete prism expansion is measured at 38 and 60 °C for 1–2 years.

2. Methods and materials

We start by presenting the overall methodology for determining the alkali metal distribution in the cement paste. The following sections describe the material characterization and experimental methods used to provide input for the methodology.

2.1. Methodology for determining the alkali metal distribution in cement paste

Fig. 1 shows a flow chart for the experimental process of determining the alkali metal distribution in cement pastes with steps labelled I-VII.

I: The total alkali content of each paste was determined by X-ray fluorescence (XRF) of the raw materials (Table 1).

Table 1
Characterization of the cement, limestone, fly ash and volcanic pozzolan. Included are element compositions determined by XRF given as oxides, median particle size (d_{50}) and mass specific Blaine surface area.

Material	Portland cement	Limestone	Fly ash	Volcanic pozzolan
	[wt%]	[wt%]	[wt%]	[wt%]
SiO_2	19.61	13.21	55.07	47.37
Al_2O_3	4.72	3.33	21.55	13.71
TiO_2	0.34	0.17	0.94	1.54
MnO	0.06	0.15	0.06	0.17
Fe_2O_3	3.17	1.86	7.04	12.38
CaO	63.14	44.35	5.26	11.23
MgO	2.30	1.68	2.23	10.76
K_2O	1.10	0.75	2.10	0.26
Na_2O	0.40	0.23	0.92	1.70
SO_3	3.72	0.60	0.17	0.11
P_2O_5	0.11	0.04	0.71	0.18
LOI 950 °C	1.30	–	–	–
LOI 1050 °C	–	33.42	3.30	0.24
Sum	99.97	99.79	99.35	99.64
d_{50} [μm]	12.4	16.1	11.3	5.1
Blaine surface [m^2/kg]	453	402	450	733

II: Quantitative Rietveld refinement X-ray diffraction (QXRD) was used to determine the amount of non-reactive minerals with alkali metals (see Tables 2 and 3).

III: The amounts of Na and K in unreacted phases were determined using QXRD on the hydrated cement pastes for the amounts of unreacted clinker minerals (see Section 2.5.2 and Table 9), and mass balance for the amount of unreacted SCMs (see Section 2.6 and Table 11).

IV: Subtracting the non-reactive (II) and unreacted (III) from total (I) alkali content resulted in the "reacted/reactive" alkali metal content.

V: The concentrations of Na and K in the pore solution were determined by pore solution expression (see Sections 2.4 and 3.2). The amount of free water was determined by thermogravimetric analysis (TGA, see Section 2.5.1 and Table 8). The amount of Na and K in pore solution was found by multiplying the concentrations and volumes.

VI: Subtracting the amount of alkali metals in the pore solution (V) from the reacted alkali metals (IV) resulted in a remainder which is adsorbed on the C-A-S-H. The properties and amounts of C-A-S-H were determined using both electron microscopy (Table 10) and mass balance calculations (Table 11).

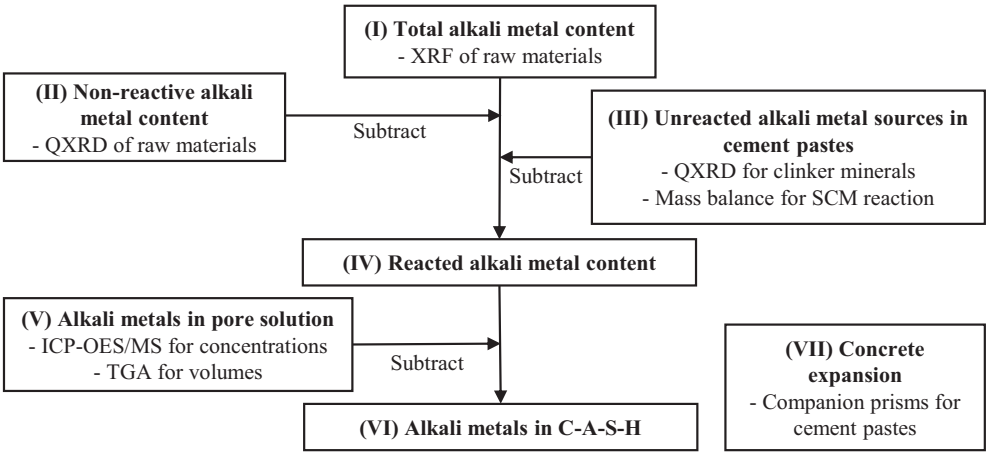

Fig. 1. Flow chart of the experimental process to determine the alkali metal distribution.

Table 2
Quantitative XRD Rietveld analysis of the Portland cement used in this study. All the phases listen in this table were considered reactive for the mass balance.

Mineral	Portland cement
	[wt%]
Alite – C_3S	60.4
Belite – C_2S	14.4
Aluminate – C_3A	7.7
Ferrite – C_4AF	8.8
Arcanite	0.2
Aphthitalite	1.5
Ca-Langbeinite	0.2
Periclase	1.2
Lime	0.4
Portlandite	0.6
Sum of clinker phases	95.5
Anhydrite	0.8
Bassanite	2.9
Gypsum	0.4
Sum of set regulators	4.1
Calcite	0.4
Sum	100.0

VII: Concrete prisms with reactive aggregates were cast and cured at 38 and 60 °C, see Section 2.7. The prisms were not used directly in the alkali metal distribution, but were used to link the findings to ASR expansion.

2.2. Raw materials

The raw materials used here are part of the NEWSCEM project. The following material characterizations were provided as parts of the project: XRF compositional analysis, X-ray diffraction (XRD) with Rietveld refinement, particle size distribution (PSD) and specific surface determined by the Blaine method. Four raw materials were used: a Portland cement (PC), limestone (L), fly ash (FA) and a volcanic pozzolan (VP).

Table 1 shows the XRF results of the raw materials used to make the cements in this project, together with the median particle diameters (d_{50}) and specific Blaine surfaces. Table 2 gives the mineral composition of the Portland cement, whilst Table 3 gives the composition of the limestone, fly ash and volcanic pozzolan. Fig. 2 shows the particle size distribution of the raw materials. The VP is notably finer than the FA, which again is similar in fineness to the limestone. To clarify the terminology, in this work we refer to all the different combinations of PC, L, FA, and VP as "cements" as a shorthand that includes both Portland cement and composite cements. All mentions of cements as normalizations such as water/cement ratio (w/c) or reported values as "per 100g cement" consistently refer to the amount of (composite) cement. Any normalization to the amount of PC or clinker are explicitly named as such.

2.3. Cement paste preparation

All cement pastes were mixed with a w/c-ratio of 0.50: A reference cement with 100 % Portland cement (PC), a limestone reference with 22 % PC replaced with limestone (PC-L), and two cements with 18 % FA or VP and 4 % limestone (PC-FA and PC-VP). Table 4 gives an overview of the cement paste proportions and abbreviations. The cement components were weighed in individual steel bowls, then combined in the largest bowl and gently pre-mixed with a steel spatula.

When mixing the cement pastes, 375.0 g deionized water was weighed in a Braun MR5550CA high shear mixer. 750.0 g cement was

Table 3
Quantitative XRD Rietveld analysis of the limestone, fly ash (FA) and volcanic pozzolan (VP) used in this study. Also indicated is which phases are considered reactive in the mass balance. Phases marked with * are solid solutions with varying composition, but the average composition used for the mass balance is given in the table.

Mineral	Chemical composition	Reactive in mass balance?	Limestone	FA	VP
			[wt%]	[wt%]	[wt%]
Calcite	$CaCO_3$	Yes	78.1	0.2	–
Belite – C_2S	Ca_2SiO_4	Yes	–	0.8	
Gypsum	$CaSO_4{\cdot}2H_2O$	Yes	0.8	–	–
Periclase	MgO	Yes	–	1.0	–
Lime	CaO	Yes	–	0.4	–
Portlandite	$Ca(OH)_2$	Yes	–	–	–
Anhydrite	$CaSO_4$	Yes	0.8	–	–
Mullite	$Al_6Si_2O_{13}$	No	–	7.0	–
Quartz	SiO_2	No	5.0	5.9	–
Maghemite	Fe_2O_3	No	–	1.6	–
Hematite	Fe_2O_3	No		0.5	
Anatase	TiO_2	No	–	0.3	–
Microcline	$KAlSi_3O_8$	No	2.3	–	–
Sanidine*	$(K_{0.5},Na_{0.5})Al(Al_{0.5},Si_{0.5})Si_2O_8$	No	1.3	–	
Anorthite	$CaAl_2Si_2O_8$	No	5.2	–	–
Augite*	$(Ca_{0.5},Fe_{0.5})(Mg_{0.5},Fe_{0.5})Si_2O_6$	No	1.9	–	2.8
Diopside*	$Ca(Mg_{0.5}, Fe_{0.5})Si_2O_6$	No	1.9	–	2.8
Amphibole*	$Ca_2(Mg_{0.5},Fe^{+2}_{0.5})_4Al(Si_7Al)O_{22}(OH_{0.5}, F_{0.5})_2$	No	1.2	–	–
Clinochlore*	$(Mg_{0.5},Fe_{0.5})_6(Si_{0.5}, Al_{0.5})_4O_{10}(OH)_8$	No	0.7	–	–
Biotite (mica)*	$K(Fe_{0.5},Mg_{0.5})_2(Si_3AlO_{10})(OH)_2$	No	1.3	–	–
Aegirine	$NaFeSi_2O_6$	No	–	–	1.1
Forsterite	Mg_2SiO_4	No	–	–	5.0
Albite	$NaAlSi_3O_8$	No	–	–	5.1
Montmorillonite*	$Ca_{0.2}(Al_{0.5},Mg_{0.5})_2Si_4O_{10}(OH)_2{\cdot}H2O$	No	0.3	–	–
Amorphous	–	Yes	–	82.3	83.2
Sum	–	–	100.8	99.9	100.0

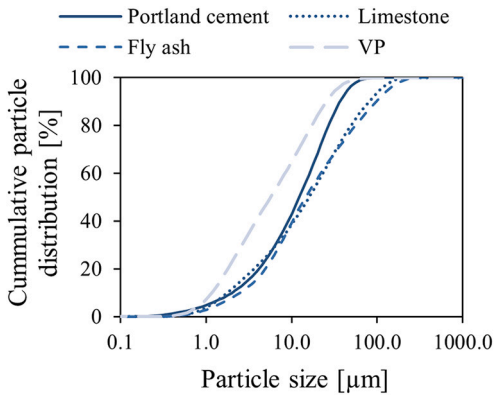

Fig. 2. Particle size distribution of the raw materials used in this study: A Portland cement, limestone, fly ash and volcanic pozzolan (VP).

Table 4
Overview of the cement pastes cast for this study.

Full name	Shorthand name	Portland cement [wt%]	Limestone [wt%]	SCM [wt %]
Portland cement	PC	100	0	0
Portland cement with limestone	PC-L	78	22	0
Fly ash cement	PC-FA	78	4	18
Volcanic pozzolan cement	PC-VP	78	4	18

then added to the mixer, then blended at medium speed (6/15) for 1 min. Whilst pausing for 1 min, a spatula was used to scrape any potential lumps stuck to the walls, bottom, or blade of the mixer. The paste was then mixed for another minute, before being distributed evenly in 3 × 125 mL and 3 × 20 mL polypropylene bottles. These were closed with lids and parafilm, then stored in closed boxes filled with deionized water. The water level was up to the bottle necks of the 125 mL bottles, whilst the 20 mL bottles were submerged. During curing the pastes were stored at constant temperatures of 20, 38 or 60 °C. The pastes were then cured for 180 days.

2.4. Liquid analyses

2.4.1. Pore solution expression

The pore solutions were expressed following the recommendations of Vollpracht et al. [32]. After curing for 180 days the cured cement pastes were cut out of the 125 mL polypropylene bottles using a knife and hacksaw, then placed in the pore solution expression kit mounted in a hydraulic press following the procedure as described by De Weerdt et al. [56]. The cell was loaded with 30 t force for 10 min, then 55 t until sufficient pore solution had been expressed (typically 2–15 min). Loads of 30 and 55 t equal pressures of 150 and 275 MPa respectively with the 50 mm diameter load cell. As the pore solution was expressed it was collected in a plastic syringe, then deposited into 15 mL centrifuge tube. Three parallel pore solution samples were expressed for each cement paste at each temperature.

2.4.2. pH measurements

Measurements of pH were performed shortly after pressing. 1–2 mL of the pore solutions were deposited in new 15 mL centrifuge tubes, in which the pH was measured using a WTW SenTix 81 electrode. The solutions were at room temperature of 22 ± 1 °C. To reduce the impact of the alkali error we measured the H^+ potentials and temperatures of the pore solutions, then used the KOH electrode recalibration described by Traynor et al. [57] to calculate the pH. This involved measuring the potential of the electrode in NaOH and KOH solutions with concentrations ranging from 0.0001 to 3 mol/L. These measurements were then correlated with pH values calculated using an extended Debye-Hückel equation to make a calibration curve. Since the pore solutions were dominated by K the KOH calibration curve was chosen over NaOH.

2.4.3. Pore solution composition

The pore solution compositions were determined using ICP-OES/MS, depending on the concentration of each element. After expression, 1 mL of the pore solutions were diluted 1:100 in volumetric flasks using mili-Q deionized water. 10 mL of the diluted solutions were deposited in a 15 mL centrifuge tube. 0.14 mL 32.5 % HNO_3 was then added to reach 1 mol/L HNO_3. This resulted in a total dilution of 1:101.4 before analysis.

Concentrations in the pore solutions were measured by Heidelberg Materials Global R&D. They used an Agilent 5110 ICP-OES and Agilent 7800 ICP-MS to determine the concentrations of Na, Al, Si, S, K and Ca. ICP measures each element without providing information about the dominant ionic species. In solution Na and K are predominantly present as Na^+ and K^+. When discussing alkali metal content in the pore solution, the reader should consider these two representations as equivalent.

2.5. Solid analyses

All methods for solid analysis were based on the recommendations found in "A practical guide to microstructural analysis of cementitious materials" [58]. One of the 20 mL bottles with cement paste was used to extract samples for XRD, TGA and SEM. The bottle was cut into slices using a IsoMet 1000 Precision Saw cooled with water. A 6 mm thick slice from the middle of the bottle was used for solvent exchange, and a 3 mm slice was placed in 2-propanol whilst waiting for SEM polishing.

The 6 mm slice was coarsely ground in a porcelain mortar until it passed a 1 mm sieve, then placed in a vacuum filtration unit. 100 mL 2-propanol was added, then stirred for 30 s. The mix was left for 5 min, then filtrated until dry. This was repeated with another 100 mL of 2-propanol, then finally with 20 mL diethyl ether. After filtrating till dry, the powders were stored overnight or over the weekend in a vacuum desiccator at 0.8 bar. The following workday they were ground in porcelain mortars until passing a 63 µm sieve. These ground powders were used for TGA and XRD measurements the same day.

2.5.1. Thermogravimetric analysis

Approximately 200 mg of the cement pastes after solvent exchange were placed in 600 µL alumina crucibles. These were then heated in a Mettler Toledo TGA/DSC 3+ from 40 to 900 °C, with a heating rate of 10 °C/min. Whilst heating, the specimen chamber was purged with N_2 at 50 mL/min.

The TGA results were used to determine Portlandite (CH) and bound water content of the cement pastes. Using the derivative of the mass loss curve (DTG), the mass loss peak between 420 and 520 °C corresponds to dehydration of CH. Two estimates for the CH content were found by integrating the derivate mass loss peak, and by using a vertical step on the mass loss curve. The amount of bound water was determined as the mass loss from 40 to 550 °C. Correspondingly the amount of free water in each paste was calculated as the amount of water added minus the bound water. The CH and water content of the paste is commonly reported in terms of grams per 100 g cement. This is found by normalizing to the dry mass of the cement paste at 550 °C, the temperature at which all water is evaporated.

2.5.2. X-ray diffraction

The solvent exchanged pastes were analysed with a Bruker AXS D8 Focus XRD, equipped with a Lynxeye detector, using a CuKα source (λ = 1.54 Å) and a slit size of 0.2 mm. Each scan swept from 5 to 55°2θ over 45 min, with step size 0.01°2θ and sampling time 0.5 s per step. The pastes cured at 20 and 38 °C were front loaded into the XRD sample

holders, whereas the pastes cured at 60 °C were back loaded to reduce the impact of preferential orientation.

QXRD with TOPAS5 from Bruker was used to provide the quantities of unreacted clinker minerals, plus a selection of key hydrated phases such as CH and ettringite [59]. An external standard of quartzite was used as reference for the QXRD, which was calibrated using a NIST silicon powder standard (640d). Sample displacement was refined, and the background was calculated with the Chebychev polynomial of the 5th order. For the quantified crystal phases the scale factors and the unit cell parameters were refined. The crystallite size was refined within reasonable limits for min and max values. To calculate the degree of reaction of the clinker phases the following structures have been used for the calculations; Alite (ICSD code: 94742), Belite [60] (ICSD Code: 81096), C_3A cub. (ICSD Code: 1841), C_3A orth. (ICSD code: 100220), C_4AF (ICSD code: 51265).

2.5.3. Scanning electron microscopy

To make polished sections for SEM-EDS, the 3 mm thick paste discs were cut into smaller pieces. They were then cast in 30 mm epoxy discs (Epoxy technology, EPO-TEK 302 8OZ) using a Buehler Cast N' Vac 1000 with a pressure of 1–2 mbar. Up to four cement pastes were cast into the same epoxy disc, using the same type of cement paste cured at different temperatures. After hardening, the discs were manually polished with sandpaper of increasing fineness, with diamond spray abrasive and ethanol as the lubricant.

A Hitachi S-3400N Zeiss SUPRA-55 VP scanning electron microscope (SEM) with an Oxford Instruments X-Max 80 mm^2 energy dispersive spectrometer (EDS) was used to characterize C-A-S-H in the cement pastes. EDS point scans of inner and outer product were acquired with a beam voltage of 15 kV and working distance of 10 mm. For each paste some 150 points were acquired, and the inner product points were used to graphically determine the C-A-S-H composition as described by Scrivener et al. [61]. The composition is described by its Ca/Si and Al/Ca ratios, whereas adsorption of ions is represented by S/Si, Na/Si and K/Si ratios. Further details on these characterizations can be found in the PhD thesis of Pamela Zuschlag [62].

2.6. Mass balance

A mass balance was set up to calculate the mass of phases formed in the cement pastes. Fig. 3 shows a flow chart for the calculations, with experimental input a-f and calculation steps I-VIII, described below.

I: For each paste the total oxide composition of the cement was calculated using the proportions of the cement mixes (Table 4) and the XRF characterization of the raw materials (a, Table 1).
II: QXRD of the raw materials (b, Tables 2 and 3) was used to determine the amount of each element present in non-reactive mineral phases (also Table 3). These amounts were subtracted from the total cement composition (I). This was done by multiplying the amount of each phase with its chemical composition. As an example, microcline ($KAlSi_3O_8$) in limestone consists of 14 % K, 10 % Al, 30 % Si, and 46 % O by weight. Multiplied with the 2.3 wt% microcline in limestone means that around 0.3 % of the limestones mass is K bound in microcline. For phases with solid solutions (e.g. biotite) an average composition was used, such that (Na_{1-x},K_x) would be ($Na_{0.5}$,$K_{0.5}$).
III: QXRD of the hydrated pastes (d, Table 9) was used to determine the amount of clinker minerals remaining. The amount of each element used to compose these minerals were subtracted from the total cement composition (I). We used a modified version of the clinker mineral compositions from Taylor [6] (Table 6). More details on this can be found in the supplementary data.
IV: Subtracting non-reactive minerals (II) and unreacted clinker (III) from the total cement composition (I) gave the remainder which we call "reacted" or "reactive" cement composition. Water was added to the model in proportion to the w/c-ratio 0.50 used for the cement pastes.

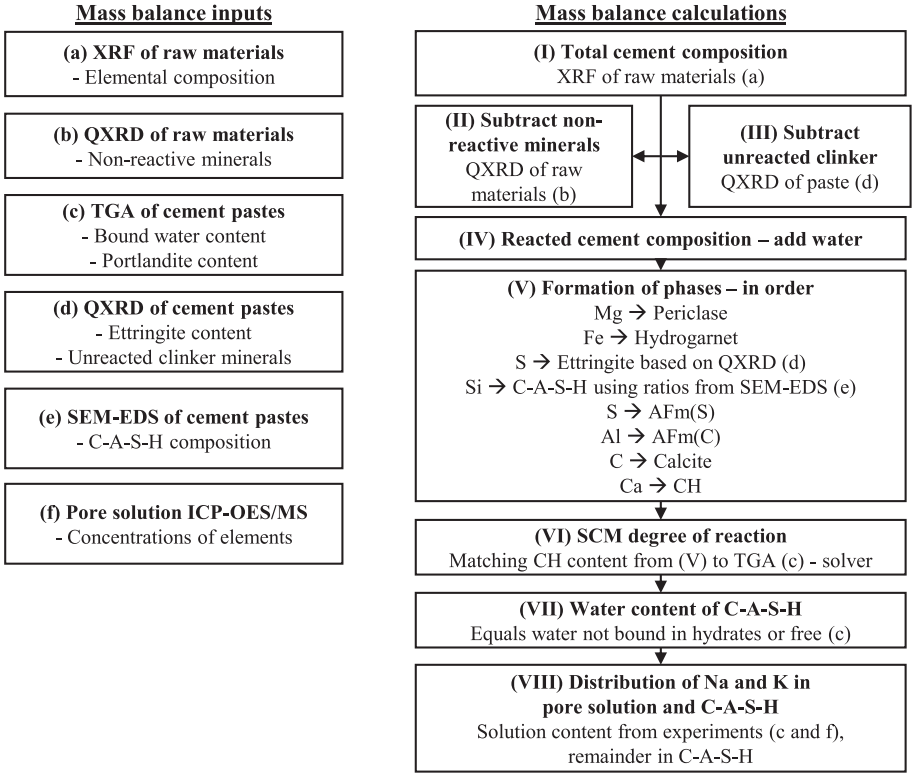

Fig. 3. Flow chart for the calculations in the mass balance. The experimental inputs are labelled a-f, and the calculation steps I-VIII. The relevant experimental input for each step of the calculation is indicated with the letter in parentheses.

V: A series of phases was formed, and the resulting amounts of elements in each phase was subtracted from the reacted cement composition (IV). The amount of ettringite was based on QXRD of the cement pastes (d, Table 9). All Si not included in hydrogarnet was used to form C-A-S-H. Experimental atomic ratios from SEM-EDS for the C-A-S-H (e, Table 10) were used to determine how much Ca, Al and S should be subtracted from the reactive composition and placed in C-A-S-H. The amount of Ca was found my multiplying the moles of Si with the Ca/Si ratio, then the amount of Al was found by multiplying the amount of Ca with the Al/Ca ratio etc.

VI: For the PC and PC-L pastes the calculated CH content from mass balance was compared to the experimentally determined content (c, Table 8) as a check for the models' accuracy. For the pastes with FA and VP, a minimization algorithm (excel solver) was used to find the degree of SCM reaction that would make the calculated CH content equal to the measured CH content. A solver function had to be used since changing the degree of hydration resulted in changing the amount of C-A-S-H, thereby again changing the calculated amount of CH in the mass balance.

We only used one reactive composition for the SCMs (Table 6), thereby assuming congruent dissolution, which is a simplification of the SCM reaction. In FA we might in reality expect different populations of amorphous phases that react at different rates [63,64]. Zuschlag [62] compared the mass balance approach described above to the degree of reaction obtained by SEM image analysis for the paste samples cured at 20 and 38 °C. She found that both methods yielded similar results, thereby validating that the CH method can be used to determine the degree of reaction of these SCMs.

VII: The amount of bound water was determined using TGA (c, Table 8). The amount of free water in the pore solution was then calculated by subtracting bound water content from the total water content. During the sequential mass balance calculations the bound water content was divided among the different hydrates. Once all other hydrates had been accounted for, remaining water assumed to be part of C-A-S-H. Any reacted elements not incorporated in hydrates were assumed to be in the pore solution.

VIII: Na and K were treated uniquely in the model. Before step (IV), the amounts of Na and K in the pore solution were found by multiplying the concentrations (Table 12) and volumes (Table 8) of the pore solutions. These amounts were subtracted from the "reactive" composition (IV). Having subtracted the alkali metals in pore solution, non-reactive minerals (II), and unreacted phases (III), the remaining amounts were assumed to be adsorbed on C-A-S-H.

The excel sheet with input and calculations for the mass balance will be made available as supplementary data.

Tables 5, 6 and Fig. 4 combined show how Na and K were treated in the mass balance. The total amount of Na and K in each component in Fig. 4 was determined using XRF (Table 1). The non-reactive composition in Table 5 corresponds to non-reactive minerals in Fig. 4, which again were based on QXRD (Table 3) in a similar approach as Kalina et al. [11] who reported similar minerals in perlite and vitric ash. VP and FA are notably different in that FA has no non-reactive minerals, whereas VP has a large portion of its Na bound in aegirine and andesine.

The reactive composition in Table 5 thus corresponds to the sum of the three other parts: Alkali sulphates, other crystalline phases, and amorphous phases. The amounts of alkali sulphates was determined by QXRD (Tables 2 and 3). We used "other crystalline phases" as a catch-all for the difference in Na and K content between XRF and QXRD characterizations of PC and L, as these materials did not have any amorphous component. These "other crystalline phases" in PC are mainly the clinker minerals, which contain some alkali metals as impurities (see Table 6). This approach meant that the majority of Na in PC was considered to be part of the clinker minerals, not in alkali sulphates. Similarly for L there was very little Na in minerals compared to the amount measured in XRF, thus a large portion was attributed to "other crystalline phases". For the

Table 6
Composition of the clinker minerals used in the mass balance calculations (step III in Fig. 3). The values were based on those from Taylor [6], but adjusted to fit the XRF and QXRD results from the cement used in this study. The most notable changes are increased SO_3 content in alite and belite.

Oxide	Alite C_3S	Belite C_2S	Aluminate C_3A	Ferrite C_4AF
	[wt%]	[wt%]	[wt%]	[wt%]
CaO	71.90	62.83	59.40	44.62
SiO_2	24.13	31.11	3.70	3.60
Al_2O_3	0.97	2.07	27.40	19.71
Fe_2O_3	0.73	0.91	5.27	24.90
MgO	1.02	0.50	1.38	2.92
SO_3	0.81	0.88	0.00	0.00
Na_2O	0.16	0.12	1.81	0.11
K_2O	0.12	1.23	0.81	0.21
P_2O_5	0.16	0.11	0.00	0.00
TiO_2	0.00	0.24	0.22	3.26
Mn_2O_3	0.00	0.00	0.00	0.68
Sum	100.00	100.00	100.00	100.00

Table 5
Relating to Fig. 3, the table shows the composition of the non-reactive (II) and reactive parts (IV) of the raw materials. The non-reactive composition was calculated using the QXRD results of the materials. The reactive composition was found by subtracting the non-reactive composition from the total composition as determined with XRF (Table 1). These values were used for further calculations in the mass balance, and likely do not have the number of significant figures indicated by the table.

Element	Non-reactive composition				Reactive composition			
	PC	L	FA	VP	PC	L	FA	VP
	[wt%]	[wt%]	[wt%]	[wt%]	[wt%]	[wt%]	[wt%]	[wt%]
C	0.00	0.00	0.00	0.00	0.35	9.12	0.90	0.11
Si	0.00	6.02	3.65	4.24	9.17	0.16	22.09	18.10
Al	0.00	1.66	2.66	0.52	2.50	0.10	8.75	7.08
Ti	0.00	0.00	0.19	0.00	0.20	0.10	0.37	0.92
Mn	0.00	0.00	0.00	0.00	0.05	0.12	0.05	0.13
Fe	0.00	1.18	1.51	1.26	2.22	0.12	3.42	7.06
Ca	0.00	1.36	0.00	0.72	45.13	30.34	3.76	7.75
Mg	0.75	0.44	0.55	2.03	0.64	0.57	0.80	3.50
K	0.00	0.53	0.00	0.00	0.91	0.09	1.74	0.26
Na	0.00	0.05	0.00	0.56	0.30	0.12	0.68	0.79
S	0.00	0.00	0.00	0.00	1.49	0.24	0.07	0.01
P	0.00	0.00	0.00	0.00	0.05	0.02	0.31	0.07
O	0.50	9.85	7.66	7.51	35.73	37.60	40.20	36.88
Sum	1.25	21.10	16.22	16.84	98.72	78.66	83.13	82.67

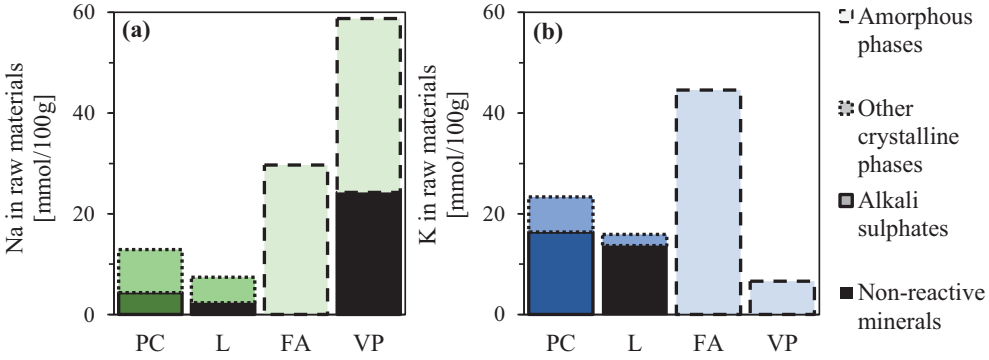

Fig. 4. Calculated distribution of Na (a) and K (b) in the raw materials, based on XRF (Table 1) and QXRD (Tables 2 and 3) of the raw materials.

sake of the mass balance, this fraction of Na and K were assumed to be reactive.

The final fraction was then the amorphous content of FA and VP, which is known to contain reactive Na and K [11,63]. As with "other crystalline phases" in PC and L, we assumed that the difference between the Na and K in crystalline phases from QXRD and the total amount from XRF represents the amounts in the amorphous phase. Here we also used a simplified assumption of congruent dissolution of the amorphous phase, meaning the amount of Na and K released is proportional to the overall degree of SCM reaction.

2.7. Concrete performance testing

The concrete recipes used for ASR performance testing is given in Table 7. In each case the cement is identical to those used in the cement pastes: 78 % Portland cement, 4 % limestone and 18 % SCM. The concretes had cement contents of 445–450 kg/m^3, and water to cement ratio of 0.48. A blend of non-reactive fine, reactive fine, and highly reactive coarse aggregate was used: Årdal innocuous sand (0/4 mm, 415–420 kg/m^3), Søberg reactive sand (0/10 mm, 345–350 kg/m^3) and Ottersbo reactive gravel (4/16 mm, 960–980 kg/m^3). Årdal is a natural sand mainly composed of gneiss and granite. Søberg is a natural sand/gravel composed of different rock types, mainly gneiss, greenstone, shist, rhyolite, quartzite, amphibolite and gabbro. Ottersbo is a crushed cataclasite with crypto and micro-crystalline quartz. This is a Norwegian reference reactive aggregate used for documenting the mitigation properties of composite cements with SCMs.

SINTEF performed the ASR performance testing according to the Norwegian 38 °C Concrete Prism Test (NCPT) [65] and RILEM AAR-11 60 °C CPT [66]. The NCPT is comparable with the recently published RILEM AAR-10 [40] concrete performance test (except for small deviations in the concrete composition). For each composite cement a set of three 100x100x450 mm concrete prisms (NCPT) and three 70x70x280 mm (RILEM AAR-11) were prepared for testing. To check the concrete quality (see Table 7), the freshly mixed concrete was tested according to EN 12350 for slump, density, and air content. Three 100 mm cubes for determination of 28 days compressive strength were cast for each mix and tested according to EN 12390.

After casting, the 100 mm concrete prisms (NCPT) were kept in the moulds in air at 20 ± 2 °C, 100 % relative humidity (RH) for 23 ± 0.5 h and 0.5 h in water at 20 °C prior to determination of reference length. The prisms were thereafter stored in containers over water with 100 % RH at 38 ± 2 °C for 2 years. Weight and length measurements were performed after 1, 4, 8, 16, 26, 52, 78 and 104 weeks of exposure. The length change compared to the reference length was calculated. All length measurements were performed at 20 °C, and the prisms were kept in the containers at 20 °C for 16 ± 4 h prior to each measurement.

After casting, the 70 mm concrete prisms (RILEM AAR-11) were kept in the moulds in air at 20 ± 2 °C, 100 % RH for 23 ± 0.5 h. The prisms were thereafter stored in containers over water inside a reactor with 100 % RH at 60 ± 2 °C for 1 year. The reference length was determined after about 24 h of storage at 60 ± 2 °C. Weight and length measurements were performed after 1, 4, 13, 26, 39 and 52 weeks of exposure. The length change compared to the reference length was calculated. All

Table 7
Recipes for the concrete mixes used for performance testing. The mixes are named after the cement used, which are the same cements as those used for cement pastes: Portland cement (PC), PC with 22 % limestone (PC-L), PC with 18 % fly ash and 4 % limestone (PC-FA), and PC with 18 % volcanic pozzolan and 4 % limestone (PC-VP). The compressive strength was measured on 100 mm cubes after 28 days curing.

Cement	PC	PC	PC-L	PC-L	PC-FA	PC-FA	PC-VP	PC-VP
	38 °C	60 °C	38 °C	60 °C	38 °C	60 °C	38 °C	60 °C
Na_2O in composite cement [kg/m^3]	1.8	1.8	1.6	1.6	2.2	2.2	2.9	2.9
K_2O in composite cement [kg/m^3]	4.9	4.9	4.6	4.6	5.7	5.7	4.2	4.2
Na_2O from clinker [kg/m^3]	1.8	1.8	1.4	1.4	1.4	1.4	1.4	1.4
K_2O from clinker [kg/m^3]	4.9	4.9	3.8	3.8	3.8	3.8	3.8	3.8
Cement [kg/m^3]	448	444	447	447	448	448	447	447
0–10 Søberg [kg/m^3]	349	347	348	348	343	343	346	346
0–4 mm Årdal [kg/m^3]	421	417	418	418	413	413	416	416
4–16 mm Ottersbo [kg/m^3]	979	971	974	974	973	962	969	967
Admixture C [kg/m^3]	0.7	0.77	0.7	0.81	0.4	0.78	0.7	0.83
Free water (w) [kg/m^3]	215	213	215	215	215	215	215	215
Absorbed water [kg/m^3]	8	8	8	8	8	8	8	8
w/c [-]	0.48	0.48	0.48	0.48	0.48	0.48	0.48	0.48
Slump [mm]	160	195	185	205	155	200	200	200
Air content [volume%]	1.7	1.7	1.3	1.3	1.2	1.0	1.7	1.5
Density [kg/m^3]	2420	2400	2410	2410	2390	2390	2400	2400
Compressive strength [MPa]	59.0	62.8	49.3	49.8	50.5	54.4	56.5	55.1

length measurements were performed at 20 °C, but without pre-cooling the prisms. To avoid influence of temperature deviations, a detailed test procedure was followed for all the length measurements.

3. Results

3.1. Concrete performance testing

Fig. 5 shows the ASR expansion curves of the concrete prisms stored at 38 and 60 °C. As expected, for all cements the rate of reaction is highest at 60 °C. At both temperatures the PC concrete expanded rapidly, breaching the 1-year expansion limit of 0.03 % after only a few weeks. PC-L expanded at nearly the same rate as PC at 38 °C, but slower at 60 °C. At 38 °C, both PC-FA and PC-VP appear to sufficiently suppress expansion, but PC-FA seems to be more efficient. The same trend is also found at 60 °C. PC-VP follows a similar curve of expansion as PC-FA, but again expands slightly more to the point of just exceeding the expansion limit after 26 weeks of exposure.

3.2. Pore solution

Table 12 in "Appendix A: Pore solution analysis results table" shows the concentrations measured by ICP-OES/MS and the pH of the cement paste pore solutions. Fig. 6 shows the ICP data in bar diagrams, with one subfigure for each element. The included error bars are standard deviations of results from three parallel samples. Fig. 7 shows the pH of the samples, as determined by recalibrating results with KOH according to [57], with errors bars of one standard deviation. It also includes a calculation of the OH^- concentration for each pore solution. It was calculated using the pore solution concentrations, assuming that the elements in solution were primarily the following ionic species: Na^+, K^+, Ca^{2+} and SO_4^{2-}. Al and Si were neglected in these calculations since their concentrations were vanishingly small in comparison to the other elements. The calculations also neglect the concentration of H^+ since it is on the order of 10^{-13} to 10^{-14} mol/L in the pore solutions.

PC and PC-L showed similar concentrations of Al at 38 and 60 °C, but PC had more than twice the concentration of PC-L at 20 °C. PC-FA showed the highest concentration of all measurements at 20 °C, but with significantly larger deviation between parallel samples. PC-VP was similar to PC-FA but with slightly lower values at 38 and 60 °C.

For the Ca concentrations, PC and PC-L were very similar, both with nearly equal values at 20 and 38 °C but increasing ca. 50 % going to 60 °C. PC-FA showed a decrease going from 20 to 38 °C, and then an increase going to 60 °C. As with Al, the concentration for Ca in the PC-FA-sample had a much larger standard deviation than the other samples. PC-VP showed more similar trends to PC and PC-L, here with a near doubling in concentration going from 38 to 60 °C.

The concentrations of K were highest for the PC samples, which had the maximum value near 630 mmol/L at 20 °C, with lower values near 550 mmol/L at 38 and 60 °C. The other cement showed little effect of temperature on the K concentration. PC-L was around 400 mmol/L, showing a clear decrease upon partial replacement of clinker. PC-FA had a concentration near 310 mmol/L and PC-VP around 270 mmol/L, showing that the SCMs reduce the concentration more than the limestone filler.

Like for K, the concentration of Na is higher in PC (250–260 mmol/L) than in PC-L (180–210 mmol/L) and PC-FA (160–190 mmol/L). However, the concentrations in the PC-VP samples (210–280 mmol/L) are larger than PC-L and PC-FA for all temperatures. There is also an increase with increasing temperature, where the concentration surpasses the PC cement at 60 °C.

The concentration of S has consistent trends of massive increase with temperature for all samples, consistent with the literature [31,32]. The jump is largest from 38 to 60 °C, increasing threefold for PC (62 to 195 mmol/L) and almost four times for PC-VP (38 to 142 mmol/L). There is a similar trend as for Na, where the S concentrations is lower for PC-FA than PC-L, with PC having the highest values. PC-VP had concentrations closer to those of PC-L than PC-FA, and a comparatively high concentration of 142 mmol/L at 60 °C.

The Si concentrations for PC showed a decrease from 0.44 to 0.26 mmol/L with increasing temperature from 20 to 60 °C. For the same temperature change, the concentration of Si in the PC-L pore solutions did not change. For PC-FA the concentrations at 20 and 38 °C were similar but decreased from 0.90 to 0.55 mmol/L going from 38 to 60 °C. PC-VP has lower concentrations than PC-FA but the same trend. The Si concentration decreased from 0.54 to 0.42 mmol/L with the increasing temperature from 38 to 60 °C.

The pH measurements have consistent temperature trends, where the pH decreases with increasing temperature for all pastes. PC has the highest pH, followed by PC-L, then PC-FA and PC-VP have similar values. VP had a slightly lower pH than PC-FA at 60 °C (13.25 versus 13.29). During measurements the pore solutions were at room temperature, which ranged from 20.5 to 23.3 °C. The general trends of changes in pH with temperature are also reflected in the calculated concentration of OH^-. The calculations show that the decrease in pH with increasing temperature is largely caused by the increasing concentration of SO_4^{2-}.

3.3. Solid analysis

3.3.1. Thermogravimetric analysis

Figs. 19 through 22 in "Appendix B: Thermogravimetric analysis results" show the mass loss with increasing temperature (TG) and its derivative (DTG) for the cement pastes, with one figure per curing temperature. The DTG-curves were smoothed by selecting 1/30 data

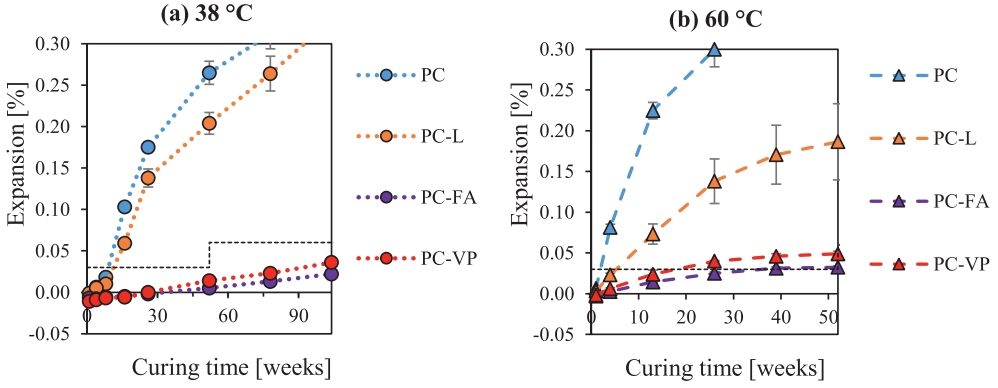

Fig. 5. Expansion of concrete prisms over time in the Norwegian CPT ((a), 38 °C) and RILEM AAR-11 ((b), 60 °C). Expansion limits are indicated with the black dashed line. For the Norwegian CPT the limits are given in the current Norwegian ASR regulations [37], whilst for RILEM AAR-11 the limit is a previous tentative limit (after about 20 weeks of exposure) recommended by RILEM (in the case of lacking national experiences based on relevant field conditions).

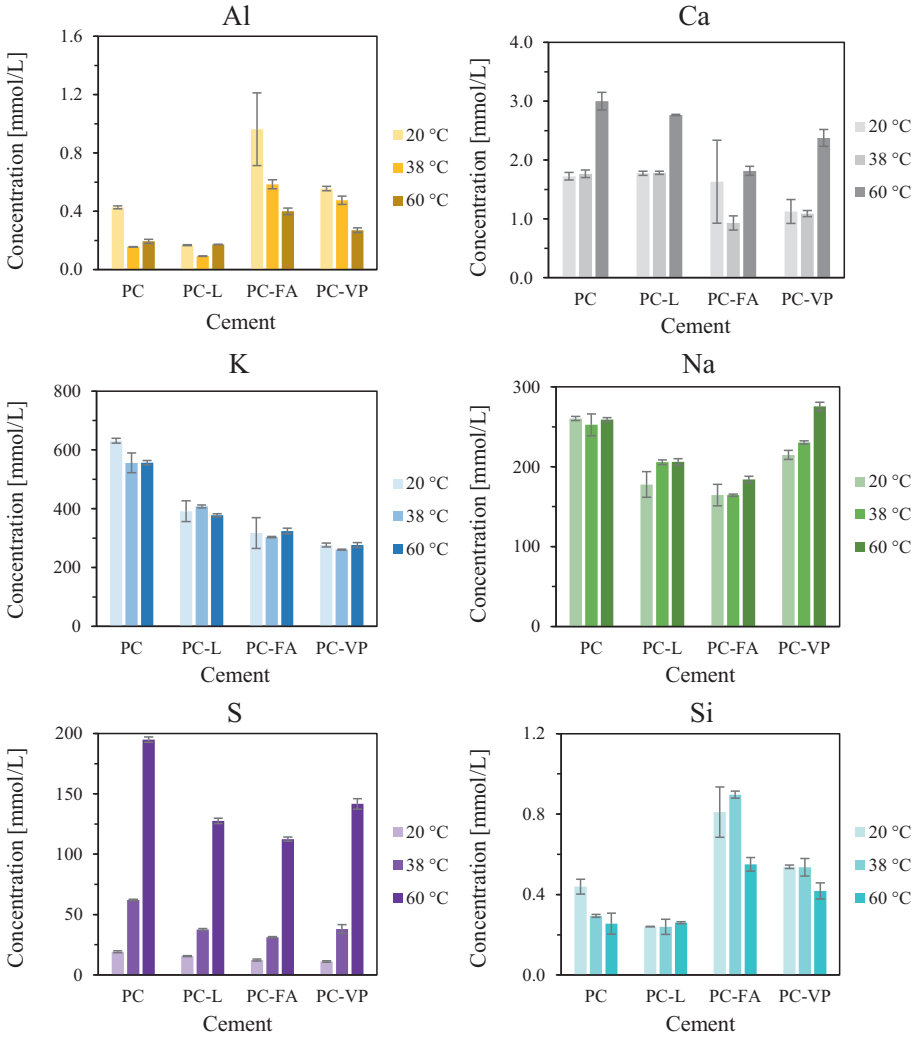

Fig. 6. Pore solution data from ICP-OES/MS, arranged with one subfigure per element. The results are grouped first by cement and then by temperature. Error bars represent standard deviations of three parallel samples.

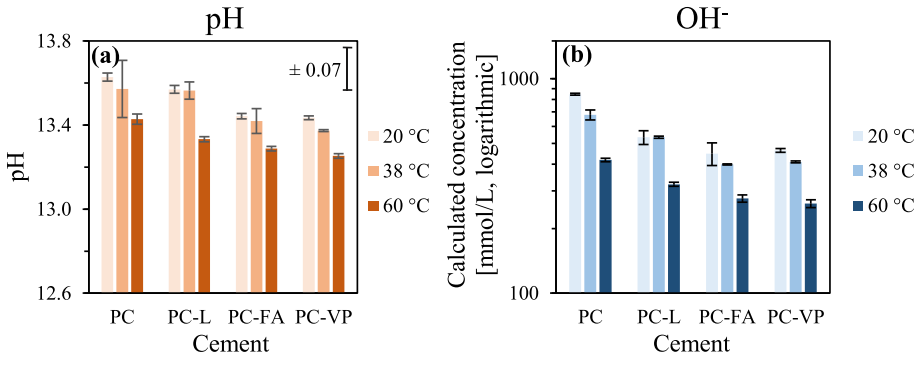

Fig. 7. pH measurements of the cement paste pore solutions (a) and the concentration of OH^- calculated with a charge balance (b). The pH measurements are averages of three parallel samples with included error of one standard deviation. Also included is a representative error associated with each individual pH measurement of ±0.07, as suggested by Traynor ea. [57]. The OH^- concentrations have error bars calculated from the standard deviation of all the elemental concentrations (Table 12 and Fig. 6) using Gaussian error propagation. Subfigure (b) uses logarithmic scale for the y-axis for more direct comparison to the logarithmic pH scale in figure (a).

points from the TG curve.

At 20 °C the PC-FA and PC-VP pastes have almost overlapping TG and DTG curves, indicating that the two pastes have similar hydrate assemblages. PC-L, PC-FA and PC-VP have similar mass loss from 40 to 160 °C. They share a distinct mass loss peak from 160 to 190 °C that is not visible for PC. PC has a unique mass loss peak from 250 to 325 °C. The Portlandite mass loss peak from 425 to 530 °C is largest for PC, followed by PC-L, then similar for PC-FA and PC-VP. The carbonates burned off above 600 °C show that PC-FA and PC-VP contain similar carbonate phases. The large mass loss from PC-L in this high temperature region comes from the decomposition of limestone (mostly $CaCO_3$) which made up 22 % of the cement.

Table 8 gives a summary of the main results from TGA, which is the amount of bound water and the Portlandite content. The Portlandite content was calculated using both the integrated DTG-peak and by using a vertical step of the TG curve. Integration typically underestimates the content, whilst vertical step overestimates. Bound water appears to decrease with increasing temperature for all cement pastes. The amount

Table 8
Summary of TGA results.

Cement	Curing temperature	Bound water	Free water	Portlandite content, integral	Portlandite content, vertical step
	[°C]	[g/100 g cement]	[g/100 g cement]	[g/100 g cement]	[g/100 g cement]
PC	20	30.5	19.5	18.3	27.5
	38	27.2	22.8	19.2	29.2
	60	26.8	23.2	18.6	27.6
PC-L	20	24.5	25.5	14.9	22.2
	38	22.1	27.9	14.8	22.1
	60	21.9	28.1	13.7	20.5
PC-FA	20	26.2	23.8	10.5	17.5
	38	23.7	26.3	8.9	15.7
	60	24.0	26.0	6.3	12.6
PC-VP	20	27.7	22.3	11.4	18.2
	38	25.2	24.8	10.0	16.6
	60	24.7	25.3	7.8	15.0

of Portlandite does not appear to trend with temperature for PC and PC-L but shows a decrease with increasing temperature for PC-FA and PC-VP. This is likely due to the increased pozzolanic reaction at higher temperatures. Taylor [54] reported similar values for bound water content in PC and PC-FA.

3.3.2. X-ray diffraction

Table 9 shows the XRD Rietveld results of the cement pastes. The amounts of clinker minerals, CH and ettringite in the pastes are given as gram per 100 g cement. There are no clear trends of change in clinker mineral contents with temperature. PC-L appears to have a larger content of C_2S and lower content of C_4AF than the other pastes. The ettringite content is low for PC regardless of temperature, whilst the other pastes show a decrease with increasing temperature as ettringite is chemically destabilized. The elevated curing temperature is also likely to accelerate SCM reactivity, thereby releasing more aluminate to the system which stabilizes AFm phases. X-ray spectra for low angles 8–14°2θ are available in "Appendix C: X-ray diffraction spectra".

3.4. C-A-S-H characterization with SEM-EDS

The characterization of C-A-S-H is of great importance for the mass balance, and thereby also the calculated distribution of the alkali metals in the solid phases. We will therefore go into detail on how the SEM-EDS results were interpreted. Table 10 summarizes the C-A-S-H characterization performed by SEM-EDS, presented as atomic ratios.

Table 9
Content of clinker minerals, Portlandite and ettringite in the cured cement pastes, as determined by XRD Rietveld refinement. The amount in g/100 g cement was calculated using the bound water content found by TGA.

Cement	Curing temperature	C_3S	C_2S	C_3A	C_4AF	CH	Ettringite
	[°C]	Content in paste [g/100 g cement]					
PC	20	0.4	3.9	0.1	4.9	15.3	2.9
	38	0.0	2.1	0.8	4.9	16.8	2.2
	60	0.5	3.9	1.2	4.9	18.0	2.1
PC-L	20	0.0	6.4	0.4	2.7	13.5	6.1
	38	0.0	6.2	0.7	3.3	14.5	4.4
	60	0.3	3.5	0.8	4.2	13.6	2.2
PC-FA	20	0.0	3.6	0.0	3.6	10.2	6.1
	38	0.0	3.8	0.1	4.2	8.6	4.3
	60	1.6	2.6	0.9	4.3	6.1	1.4
PC-VP	20	0.4	3.9	0.1	4.9	11.7	6.1
	38	0.0	2.1	0.8	4.9	9.6	3.5
	60	0.5	3.9	1.2	4.9	8.3	1.4

Table 10
Summary of C-A-S-H composition used in the mass balance, as determined by SEM-EDS point scans of inner product.

Cement	Curing temperature	Ca/Si	Al/Ca	S/Si	Na/Si	K/Si
	[°C]	[atomic]				
PC	20	1.77	0.07	0.12	0.024	0.019
	38	1.64	0.05	0.12	0.021	0.014
	60	1.65	0.05	0.09	0.017	0.012
PC-L	20	1.68	0.06	0.10	0.039	0.042
	38	1.67	0.05	0.08	0.031	0.031
	60	1.40	0.06	0.06	0.023	0.008
PC-FA	20	1.46	0.10	0.06	0.020	0.027
	38	1.49	0.09	0.07	0.017	0.026
	60	1.40	0.14	0.04	0.106	0.106
PC-VP	20	1.40	0.09	0.08	0.016	0.010
	38	1.42	0.09	0.08	0.015	0.011
	60	1.40	0.13	0.05	0.116	0.043

3.4.1. Ca/Si ratio

Determining the Ca/Si ratio for the pastes cured at 60 °C proved to be more difficult than at 20 and 38 °C. At 20 and 38 °C the atomic ratio plot Al/Ca vs Si/Ca had point clouds that were grouped tightly in the rightmost corner of the C-A-S-H – CH – AFm triangle. This was also true for PC and PC-L at 60 °C, but not for PC-FA and PC-VP. Fig. 8 shows these elemental ratio plots for all pastes cured at 60 °C.

Normally the rightmost corner is used to read off the Si/Ca (and inversely Ca/Si) and Al/Ca ratios of the C-A-S-H. For Portland cements this tends to give Ca/Si-values in the range of 1.6–1.9, which we can see from Table 10 is the case for the PC and PC-L pastes at 20 and 38 °C. When Si-rich pozzolanic SCMs are included in the cement the Ca/Si is lowered to the range of 1.4–1.6. Again, we can see this with the PC-FA and PC-VP pastes cured below 60 °C. When these values were used in the mass balance, the resulting phase distribution agreed well with the CH content measured by TGA.

At 60 °C, only the PC paste fell within the expected values. Direct reading of the atomic ratio plot gave a Ca/Si ratio around 1.65, which is on the lower side for pure PC pastes. The PC-L paste appeared to have a Ca/Si ratio of 1.3, despite not containing any siliceous pozzolan. The composite cements went even further, with PC-FA having a Ca/Si ratio near 1.0 and PC-VP closer to 0.9. These values invalidated the mass balance calculations, as a large surplus of Ca is calculated to form CH even when 100 % of the SCMs react.

Since PC-L also showed this large decrease in Ca/Si ratio at 60 °C, it is not solely an effect of the SCMs. The elevated curing temperature appeared to drive down the Ca/Si ratio of the inner product for all pastes, but the effect was most extreme for the pastes where parts of the clinker has been replaced. Although these low values are unusual, they are not without precedence. Deschner et al. [52] reported Ca/Si ratios for PC pastes with 50 % replacement with FA or quartz, cured for 180 days at various temperatures. As the curing temperature was raised from 50 to 80 °C, the Ca/Si ratio of the FA paste decreased from 1.4 to 1.1. The paste with quartz showed an enormous decrease for the same temperature increase, dropping the Ca/Si ratio from 1.7 to 1.2. They suggested this might be caused by the increasing temperatures reducing the CH solubility, whilst increasing the quartz solubility. Whilst the limestone used in this study does contain 5 % quartz, it consists mostly of $CaCO_3$, not SiO_2. This implies that adding additional SiO_2 to the paste is not the only cause of lowering Ca/Si at 60 °C. It is interesting that these very different filler materials both reduce the Ca/Si ratio at extreme curing temperatures.

Our hypothesis for the low Ca/Si values is based on how the paste microstructure is greatly altered at 60 °C [31,67–71]. The TGA analysis showed that all the pastes contained a significant amount of CH. However, little to no CH appeared to be intermixed with the inner product for the PC-L, PC-FA, and PC-VP pastes. The rightmost edge of the SEM-EDS atomic ratio plot gives the composition of the extreme end of the C-A-S-

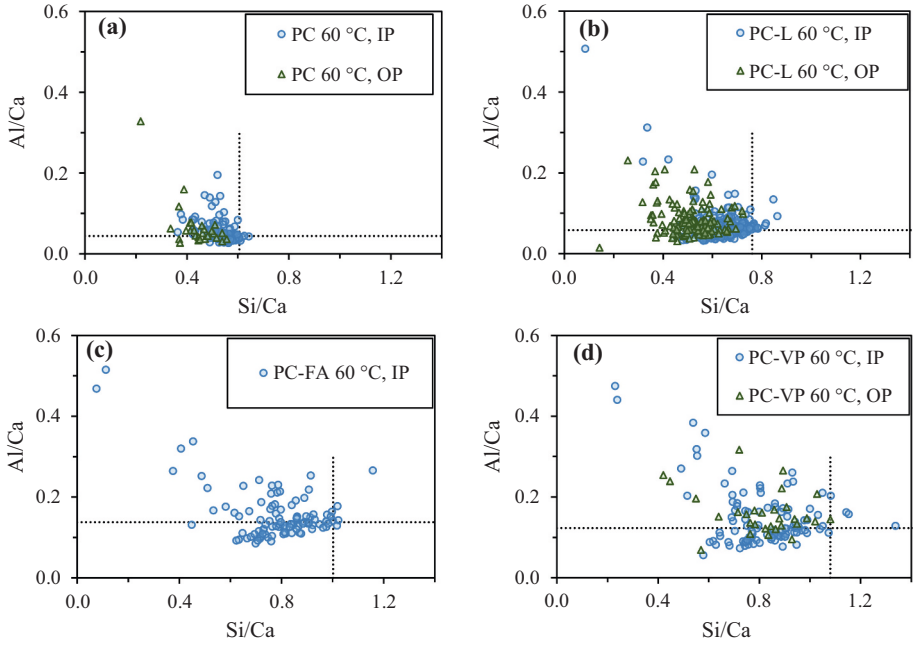

Fig. 8. Scatter plots of the atomic ratios of Al/Ca vs Si/Ca for the SEM-EDS point scans. Most of the points were acquired from inner product (IP) with some from outer product (OP). One subfigure is included per cement: PC (a), PC-L (b), PC-FA (c) and PC-VP (d). All pastes in this figure were cured at 60 °C. The dotted lines are the median values for Al/Ca (horizontal) and the 95th percentile values for Si/Ca (vertical).

H composition spectrum within the paste. It is also likely that some of the fine particles of FA and VP were intermixed with the inner product, which also contributed to lowering the Ca/Si ratio.

According to the model from Richardson [72], C-A-S-H in its pure form is limited to Ca/Si ratios between 2/3 and about 1.4. Lower values imply intermixing with amorphous silica, and higher values imply intermixing with an amorphous or poorly crystalline Ca-rich phase like CH or $CaCO_3$. Considering this model and the fact that all our pastes contain CH, we chose to use 1.4 as the lowest boundary of the Ca/Si for C-A-S-H in our mass balance.

In summary, we use the following rules to determine the Ca/Si ratio to use for C-A-S-H in our mass balance: If the rightmost edge of the Al/Ca vs Si/Ca point cloud was lower than 0.7 on the Si/Ca axis we used the 5th percentile of the measured Ca/Si ratio values. If the Ca/Si determined by this method was lower than 1.4, we instead used 1.4 as the value. We feel it is important to stress here that we are unable to measure C-A-S-H as a pure phase, and that the values presented here are in some way an average representation of C-A-S-H in the cement paste.

3.4.2. *Al/Ca and S/Si*

Rather than subjectively reading off the Al/Ca from the plots in Fig. 8, we chose to use a common criterion for all the pastes. The point clouds were scattered in such a way that the manually read Al/Ca would correspond quite well to the median value of all inner product measurements. The median value was therefore used in the mass balance.

To determine S/Si, we follow the approach used by Ben Haha et al.

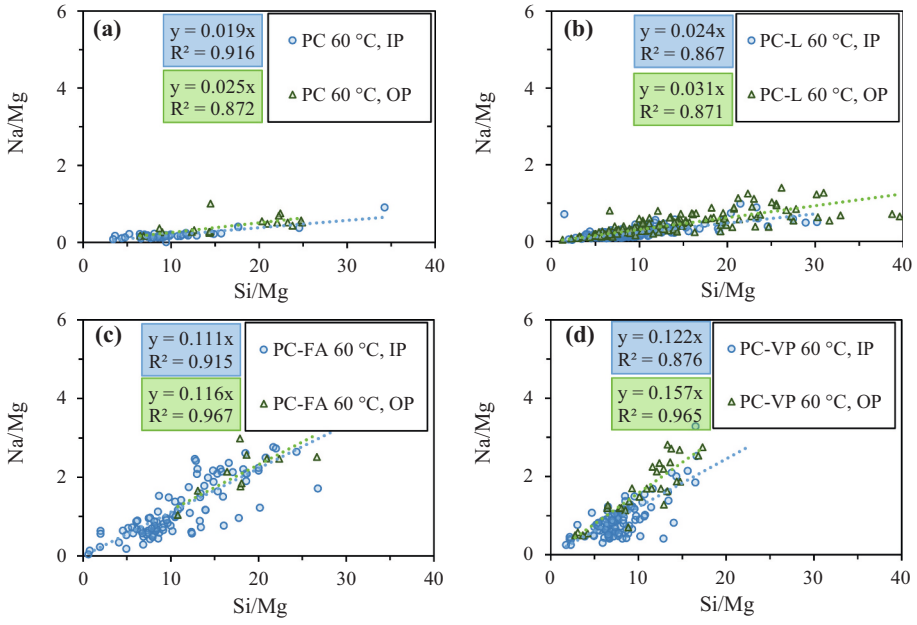

Fig. 9. Scatter plots of the atomic ratios Na/Mg vs Si/Mg for the SEM-EDS point scans of pastes cured at 60 °C. Most of the points were acquired from inner product (IP) with some from outer product (OP). One subfigure is included per cement type: PC (a), PC-L (b), PC-FA (c) and PC-VP (d). The dotted lines and coloured boxes are from linear regression lines of the IP (blue, top) and OP (green, bottom), with included slope corresponding to a Na/Si ratio. Points with 0 % Na were not included in these figures. (For interpretation of the references to colour in this figure legend, the reader is referred to the web version of this article.)

[73] and others [62,74]. We normalise the S and Si contents to an element that is not in C-A-S-H, in our case we use Mg. We then see a straight line when plotting S/Mg against Si/Mg, and the slope of this line is the S/Si of C-A-S-H. We considered the variations above and below to be mostly a measure of spread in S/Si per CA-S-H. The S/Si ratio we used for the mass balance was therefore the median value, which was very similar in value to the slope of the S/Mg vs Si/Mg plot. These scatter plots are provided as supplementary data.

3.4.3. Na/Si and K/Si

Following a similar method as with S/Si, Fig. 9 shows atomic ratio plots of Na/Mg against Si/Mg. Similar distributions also appeared for K/Mg vs Si/Mg, so we will treat both alkali metals in this section by referring to them interchangeably as (Na,K).

For all pastes there appeared to be linear trends in the distribution of points in these plots, suggesting that the slope of this distribution could correspond to the (Na,K)/Si ratio of C-A-S-H. The linearity only held when point scans with zero (Na,K) detected were filtered out. Several points appeared to have (Na,K) content below the detection limit for the SEM settings used. We found that the graphical solution described above gives a slope that is very close to the median value of (Na,K)/Si in the inner product. This median was therefore used as an estimate for the atomic ratios in C-A-S-H.

Most samples give reasonable values with this method. However, for PC-FA and PC-VP at 60 °C the (Na,K)/Si ratio is improbably high. Using PC-VP 60 °C as an example, mass balance predicts a Na/Si ratio of 0.026, whereas SEM-EDS gives 0.116. Normalizing to Ca gives similar numbers, with Na/Ca ratio of 0.018 from mass balance and 0.095 from SEM-EDS. The mass balance calculates a value that should correspond to average (Na,K)/Si throughout the entire cement paste.

There are a few possibilities as to why there is such a discrepancy between these two methods. It is possible that some alkali metal rich SCM phases are included in the EDS point. This would increase the amount of Si and (Na,K), but proportionally to the content of (Na,K)/Si in the SCM. However, the example ratios we can read from Fig. 9 are much higher than those of the SCMs. As an example, the VP has a Na/Si ratio of 0.07, yet the PC-VP paste at 60 °C has an apparent Na/Si ratio of 0.116. Intermixing with SCM therefore appears unlikely to be the only reason for the extreme (Na,K)/Si ratios.

Another explanation could be precipitation of alkali metal hydroxides or carbonates during preparation of the polished sections. If there are precipitates in the pores that have been emptied of solution, this could increase the local mass of Na or K. It could also be the case that as the pore solution was gradually removed, the Na and K concentration increased, which lead to increased binding by the C-A-S-H. It might also be the case that since the high alkali metal contents are only observed at 60 °C, there could be some phase that only precipitates at high temperature. Shi et al. [75] demonstrated that in concrete exposed to KOH solutions at 60 °C it is possible to form K-schlyokovite and ASR-P1 ($K_{0.52}Ca_{1.16}Si_4O_8(OH)_{2.84}\cdot 1.5H_2O$). It might seem unintuitive to compare products formed in concrete to those in pure cement paste. However, the SCMs we use contain reactive forms of silica exactly like reactive aggregates. There is no real difference between the silica from FA or from a rock containing amorphous silicates, besides the size of the particles. Siliceous SCMs should therefore theoretically be able to react and form ASR products, but under normal conditions they preferentially form more C-A-S-H at lower Ca/Si instead.

Regardless of what the real mechanism is, for PC-FA and PC-VP at 60 °C the numbers of (Na,K)/Si from SEM-EDS are incompatible with the mass balance. The other pastes all have values much closer to the mass balance. Table 10 summarizes the SEM-EDS characterization, using the median (Na,K)/Si for IP. However, due to the large variety of unknowns in how the SEM-EDS values are determined, we will use the values calculated with mass balance in the discussion.

3.5. Mass balance

Table 11 presents a summary of key results from the mass balance. Fig. 10 shows the phase distribution in the cement pastes calculated using the mass balance. The PC and PC-L pastes act here as checks for the validity of the mass balance calculations. For all PC and PC-L pastes (except PC-L at 60 °C) the calculated CH content agreed very well with the experimental results from TGA. PC-L at 60 °C is impacted by the difficulties of determining Ca/Si ratio as discussed in Section 3.4.1. The calculations appeared to overestimate the amount of Ca available to form CH. However, we considered the calculations to be satisfactory considering how well the model of the other PC and PC-L pastes agreed with the experimental results.

For the mass balance of the pastes containing FA or VP, as Si and Al are added to the system more C-A-S-H is formed. This results in less Ca being available to form CH. This relationship was used to determine a degree of reaction for the SCMs by minimizing the difference between the TGA results and the mass balance calculations.

Using this method yielded a degree of SCM reaction below 100 % for all pastes, indicating that the mass balance calculations are realistic. Table 11 shows these calculated degrees of reaction, presented as a percent of the total amount of SCM in the paste. Since parts of the SCMs are non-reactive minerals, the upper limit for these values is equal to the sum of reactive components presented in Table 5, ca. 83 % for both FA and VP.

The main results of the mass balance that are of interest for the alkali metal distribution are the amounts of Si in C-A-S-H, and how much of the cement components that are unreacted. Fig. 11 shows a comparison of the Na/Si and K/Si ratios calculated from the mass balance and determined by SEM-EDS (see Section 3.4.3).

4. Discussion

Here we will present how the data of pore solution and solid analyses come together in the mass balance to provide information on the distribution of alkali metals in the cement pastes. In the discussion of how Na and K are distributed, using mass is misleading due to the large difference in molar mass. We will therefore in this discussion use molar units, then convert to mass for engineering purposes at the end.

4.1. Distribution of alkali metals

4.1.1. Alkali in the unhydrated cements

Before looking at the hydrated pastes, we will consider the distribution of Na and K in the unhydrated cements. Fig. 12 shows how much the clinker, limestone, FA, and VP individually contribute to the total alkali metal content. These values are found by combining the XRF composition of each component (Table 1) with the cement mix proportions (Table 4), visually represented in Fig. 4. As shown in Fig. 4, the majority of K in PC is in readily soluble alkali sulphates. Parts of the Na are also in alkali sulphates, but the majority is present as impurities in the clinker minerals.

Since the clinker makes up 78 % of each cement, it is by far the largest contributor of Na and K. Replacing 22 % of PC with limestone only results in a 9 % decrease in Na content and 7 % decrease in K content, as the limestone also contains significant amounts of alkali metals. Fig. 4 shows that in the limestone the majority of Na is considered reactive, whereas most of the K is bound in non-reactive crystalline phases.

In the pastes with SCMs, FA and VP contribute over 30 mol% of the total alkali metal content despite being only 18 wt% of the composite cements. PC-FA has 22 % more Na and 15 % more K than PC, which is due to the high alkali content of the amorphous phase (Table 5 and Fig. 4). Again compared to PC, PC-VP has 62 % more Na and 14 % less K. Tables 3 and 5 combined show that of this increased Na content, around 40 % is bound in the non-reactive minerals aegirine and andesine.

Table 11
Summary of key results from mass balance calculations. Values replaced with "-"indicate that this is not applicable to the cements paste. PC and PC-L do not contain any SCMs, and for PC-FA and PC-VP the CH content of the mass balance was fitted to exactly match the CH content from TGA. The amounts of Na and K in pore solution were not outputs of the model, but inputs from experimental results of pore solution (ICP-OES/MS for concentrations, TGA for volume).

Cement	Curing temperature	CH from TGA	CH from mass balance	Difference in CH content	Degree of SCM reaction	Mass C-A-S-H+ adsorbed ions	Si in C-A-S-H	Na/Si in C-A-S-H	K/Si in C-A-S-H	Na in pore solution	K in pore solution
	[°C]	[g/100 g cement]	[g/100 g cement]	[%]	[%]	[g/100 g cement]	[mmol/ 100 g cement]	[atomic]	[atomic]	[mmol/ 100 g cement]	[mmol/ 100 g cement]
PC	20	27.5	28.9	6 %	–	69.5	291.6	0.025	0.034	5.1	12.3
	38	29.2	31.4	8 %	–	64.3	302.1	0.021	0.032	5.8	12.7
	60	27.6	29.5	8 %	–	61.7	290.8	0.020	0.031	6.0	12.9
PC-L	20	22.2	21.9	-1 %	–	48.4	211.6	0.029	0.032	4.5	10.0
	38	22.1	21.8	0 %	–	46.3	212.9	0.022	0.026	5.7	11.4
	60	20.5	26.6	31 %	–	44.6	226.3	0.020	0.030	5.8	10.6
PC-FA	20	17.5	–	–	42 %	60.9	295.7	0.030	0.047	3.9	7.5
	38	15.7	–	–	47 %	61.2	303.0	0.028	0.045	4.3	8.0
	60	12.6	–	–	74 %	69.5	347.4	0.027	0.046	4.8	8.4
PC-VP	20	18.2	–	–	50 %	58.1	284.2	0.031	0.042	4.8	6.2
	38	16.6	–	–	55 %	57.6	282.6	0.029	0.040	5.7	6.5
	60	15.0	–	–	81 %	65.1	322.5	0.026	0.035	7.0	7.0

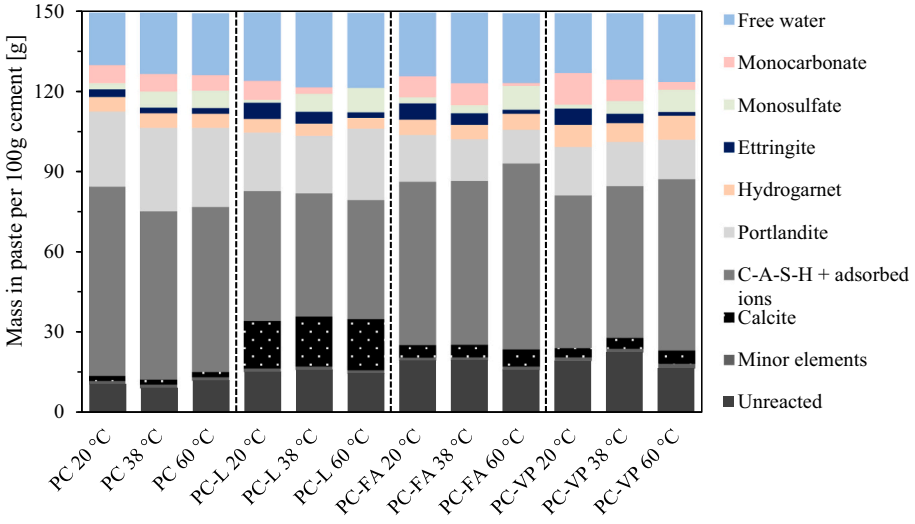

Fig. 10. Phase distribution in the cement pastes cured at 180 days, based on mass balance calculations.

4.1.2. Literature comparison

In the discussion of the alkali metal distribution determined in this study (Fig. 14) we will be comparing or findings to the closest study of this topic from literature, which is by Duchesne and Bérubé [47]. They measured the concentrations of Na and K in pore solutions of 7 pastes cured at 38 °C made with different SCMs: pulverized fly ash (PFA), condensed silica fume (CSF) and ground granulated blast furnace slag (GGBS). They then used assumptions based on literature [54] relating to release of alkali metals from ordinary PC (OPC) and SCMs, degree of reaction for the clinker and SCMs, and regarding the amount of water take up by the hydrates. With this they then calculated estimates for the distribution of Na_2O_{eq} in the pastes, which we have reinterpreted and presented in Fig. 13. In their work the word "hydrates" was used, comparatively to how we presently have used "C-A-S-H". The most direct link to the present work is in comparing their OPC to our PC, and their PFA-A and PFA-B to our PC-FA. These were however mixed with 40 % PFA, which is more than two times the 18 % FA in the present work.

4.1.3. Effect of diluting clinker

Fig. 14 shows the calculated distribution of Na and K in the hydrated cement pastes. Uncertainties are calculated using Gaussian error propagation, based on the following assumptions. For the pore solution concentrations, we use the standard deviation from Table 12. We assumed an RSD of 10 % for bound water content. These were used to find the RSD of the Na and K content of the pore solution, which are the black error bars. For the unreacted phases we assume a rather large RSD. For Na an K in unreacted clinker minerals we assume 100 % RSD, whilst we assume 50 % for the content in non-reactive limestone, unreacted FA, unreacted VP, and non-reactive VP minerals. The error bars are presented in this way to highlight the fact that the amount Na and K in C-A-S-H is calculated by subtracting the amount in pore solution and unreacted phases from the total. Therefore, the uncertainty of the amount in C-A-S-H is bounded on both sides by the uncertainty of the pore solution and unreacted plus non-reactive phases.

In the following discussion we will be referring to Fig. 14 for all values of Na/K as mmol/100 g cement (top) or as percent of total content in each cement paste (bottom). We will first consider the reference paste of PC cured at 20 °C and compare it to PC-L to show the effect of diluting the clinker. The PC contains 0.4 wt% Na_2O and 1.1 wt% K_2O, corresponding to 12.9 mmol Na and 23.4 mmol K per 100 g cement. Approximately 40 % of the Na is in the pore solution, and about 57 % is bound by C-A-S-H. Only a few percent are likely to remain in unreacted clinker, which is within the uncertainty of the method. K is distributed with 53 % in pore solution and 42 % in C-A-S-H, only 5 % remaining

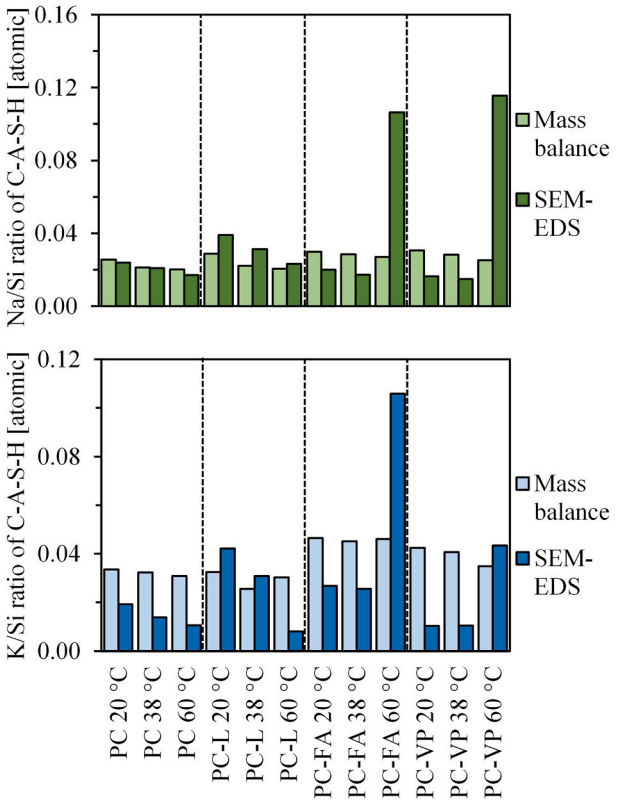

Fig. 11. Comparison of Na/Si and K/Si as calculated from mass balance and determined by SEM-EDS. The SEM-EDS values are the medians of around 100 point scans of inner product.

unreacted in the clinker minerals This agrees well with the findings of Duchesne and Bérubé [47] (Fig. 13). They assumed that all alkali metals in the PC reacted, and our findings from PC show that this was a reasonable assumption. We do however also demonstrate that there might be a difference in how Na and K distributes that is hidden when discussing Na_2O_{eq}.

The limestone used in this study has 0.2 wt% Na_2O and 0.8 wt% K_2O. Replacing 22 % of PC with limestone for the PC-L paste reduces the total Na content by 9 %, from 12.9 to 11.7 mmol/100 g cement. Similarly, total K content is reduced by 7 % from 23.4 to 21.7 mmol/100 g cement. We see then that the limestone does not "dilute" the alkali metal content of the cement in proportion to its replacement level. Limestone dilution does partially reduce the amount of available alkali metals (Fig. 12), but its main diluting role is reducing the amount of C-A-S-H that forms (Table 11). The percentwise distribution of Na in PC-L is however still similar to the PC paste, the main difference being an increase in the non-reactive fraction from 0 to 3 % and unreacted fraction from 3 to 5 %. For K, an even larger portion (14 %) is now in the non-reactive fraction, 9 % is unreacted, 32 % is in C-A-S-H and 46 % is in the pore solution.

We see that the dilution effect of replacing 22 % PC with limestone only has a minor effect on the distribution of Na. It does appear to reduce the amount and percent of K bound by C-A-S-H, potentially because of the lower concentration in pore solution and because less C-A-S-H is formed. The measured pH of PC and PC-L were similar, despite the concentrations of Na and K being higher in PC. The increase in non-reactive K from PC to PC-L is caused by the large amount of K bound in non-reactive minerals in limestone such as biotite, sanidine and microcline (see Table 3 and Fig. 4).

4.1.4. *Effect of increasing temperature*

There is a minor trend that the fraction of Na in pore solution increases with increasing temperature, going from 39 % to 47 % (PC) or 49 % (PC-L) as the temperature increases from 20 to 60 °C. A similar but much smaller trend appears for K, which goes from 53 to 55 %. This latter change is small and within the margin of error. The pore solution

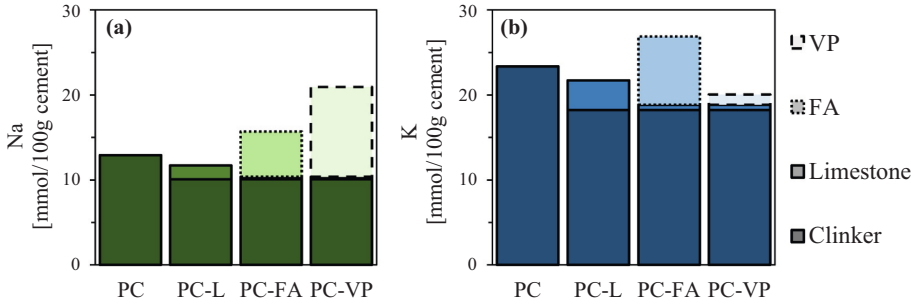

Fig. 12. Distribution of Na (a) and K (b) in the unhydrated cements used in this study, separated by cement component.

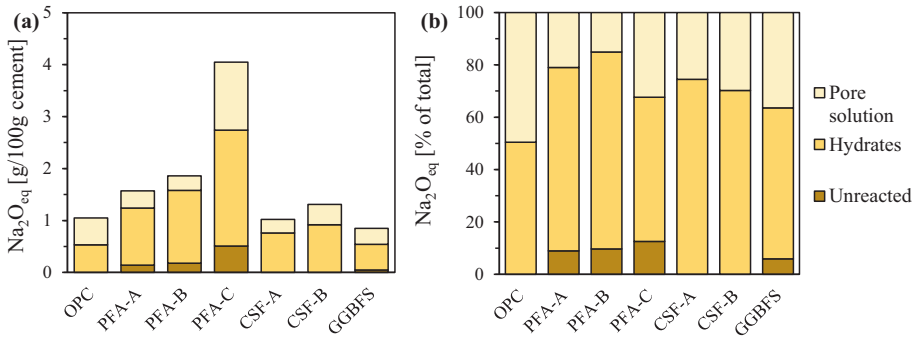

Fig. 13. Distribution of Na_2O_{eq} in hydrated cement pastes reported by Duchesne and Bérubé [47]. (a) shows the distribution in terms of total alkali metal content, and (b) shows the percentwise distribution.

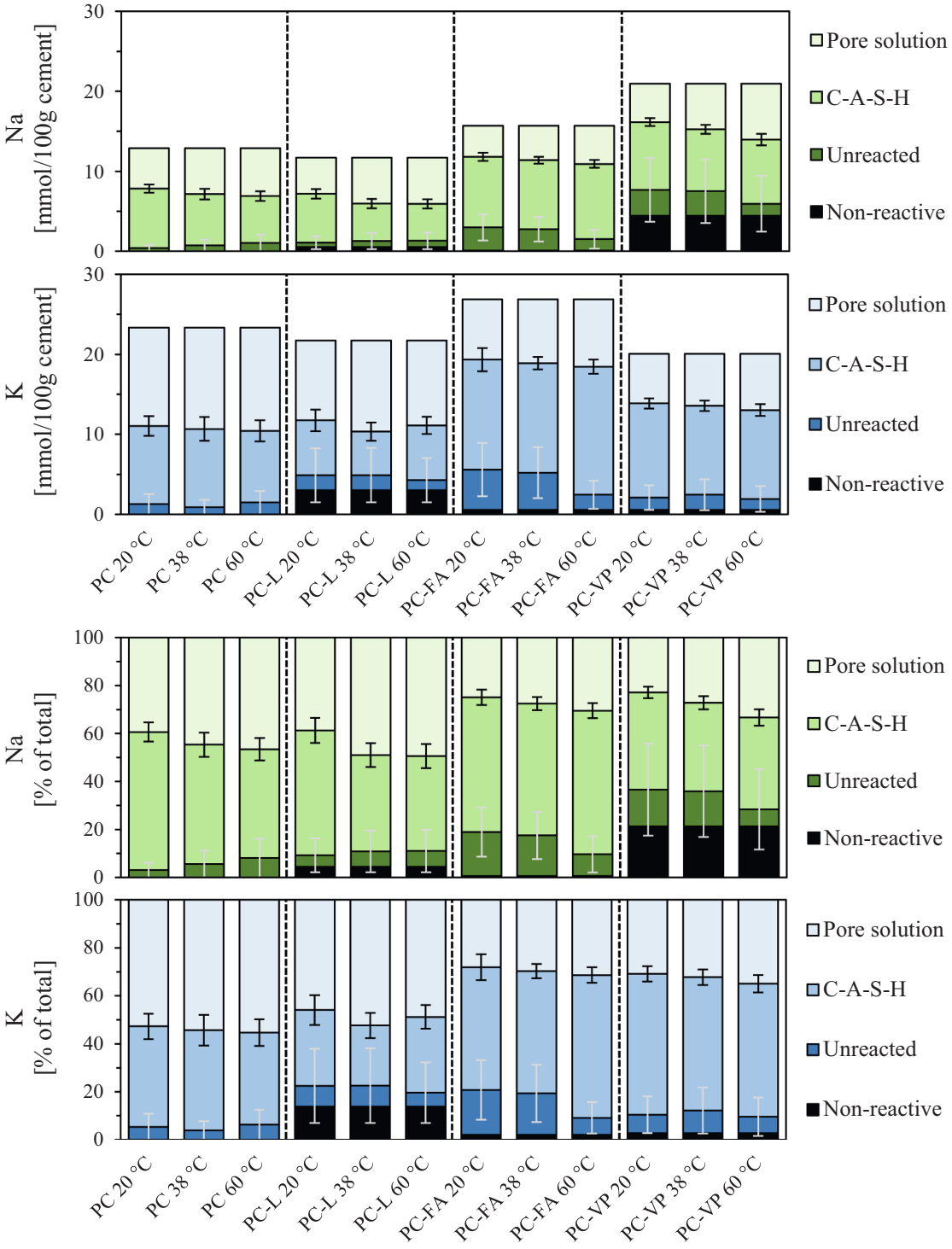

Fig. 14. Distribution of Na and K in the hydrated cement pastes. The top figure show distribution in mmol/100 g cement, whilst the lower shows distribution as percentage of total content in the cement pastes. The included errors bars are calculated with Gaussian error propagation. The black bars indicate the error of the amount of Na and K in pore solution, based on TGA and ICP-OES/MS. Light grey bars indicate the error of the amount of Na and K in unreacted plus non-reactive phases.

concentrations (Table 12) remained similar with increasing temperature. This combined with the decreasing amount of bound water (Table 8) meant that there was more solution with the same concentration, thus there was a larger total amount of Na dissolved. In summary, we find that the distributions of Na and K in PC and PC-L do not change greatly with increasing temperature. The increasing volume of free water with temperature can be linked to the lower bound water content of C-A-S-H at higher temperatures [52,67,68,70,76–78]. As an example, the mass balance calculated a molar $H_2O/(Al + Si)$ ratio for C-A-S-H in PC of 3.1 at 20 °C and 2.4 at 60 °C. In the mass balance we get these numbers as we calculate the free water amount by subtracting bound water determined with TGA from the total added water content (see Section 2.6).

Table 8 shows that the pH decreased from 13.6 to 13.4 for PC from 20 to 60 °C. This is likely caused by the increase in concentration of S, present in the solution as SO_4^{-2}. The sulphate anions counterbalance the charge of Na^+ and K^+, resulting in negative charge that is balanced by increasing the concentration of H^+. It is worth noting that the pH was measured at room temperature, and therefore does not truly reflect the pH in the cement paste at 38 and 60 °C (see "Appendix D: Influence of temperature on pore solution pH").

4.1.5. Impact of SCMs

We now compare PC-FA and PC-VP to the limestone reference PC-L cured at 20 °C. Both FA and VP contain more Na_2O than the clinker. Referring to Table 1 FA consist of 0.9 wt% and VP of 1.8 wt% Na_2O, whilst the clinker contains 0.4 wt%. The substitution of clinker with FA or VP therefore increases the Na content of the blended cement. PC-FA has a total Na content of 15.7 mmol/100 g, whilst PC-VP has 20.9 mmol/100 g.

Despite greatly increased Na content, PC-FA and PC-VP have very similar amounts of Na in the pore solution as PC-L. The difference becomes clear when comparing the percentwise distribution. PC-L has around 40 % of its Na content in the pore solution, whereas PC-FA and PC-VP have around 25 %. The three pastes have similar concentrations of Na in the pore solution. The reason for this lies in how the SCMs affect Na-binding by C-A-S-H. Both PC-FA and PC-VP have a 50 % increase in Na bound by C-A-S-H compared to PC-L, from 6 to 9 mmol/100 g cement. This corresponds to percentwise Na distributions of 52 % for PC-L, 56 % for PC-FA and 42 % for PC-VP. In addition, a larger fraction of Na remains in unreacted phases: 5 % for PC-L, 18 % for PC-FA and 15 % for PC-VP. More Na is also bound in non-reactive phases, particularly in limestone and VP. The non-reactive fraction is 4 % for PC-L, 1 % for PC-FA, and 21 % for PC-VP. This could be expected from the data in Fig. 4, which shows that 40 % of the Na in VP is in non-reactive minerals in line with the findings of Kalina et al. [11]. This reduces its effective Na contribution from 1.8 to 1.1 wt%. Comparing again to Duchesne and Bérubé [47] (Fig. 13), we find that PC-FA has a larger portion of Na and K in pore solution and unreacted plus non-reactive phases than PFA-A and PFA-B. This could be caused mostly by the different assumptions we have made regarding the release of alkali metals from the SCMs, as we have assumed congruent dissolution rather than assuming 85–100 % release of alkali metals [47].

Whereas there are some similarities of Na distribution between PC-L and PC-FA/PC-VP, the K distribution appears to be greatly affected by the SCMs. Regarding the total K content, FA has 2.1 wt% K_2O which is higher than PC (1.1 wt%), whilst the VP has 0.3 wt% which is lower. The total K-content of PC-FA is 26.9 mmol/100 g cement, which is higher than both PC (23.4 mmol/100 g cement) and PC-L (21.7 mmol/100 g cement). The PC-VP pastes contained a total of 20.0 mmol/100 g cement, which is lower than PC and PC-L.

Both PC-FA and PC-VP have lower amounts of K in the pore solution, both in terms of absolute amount and as a percent of total content. PC-L has 10.0 mmol/100 g cement in pore solution (46 % of total), PC-FA has 7.5 mmol/100 g (28 %) and PC-VP has 6.2 mmol/100 g (31 %). Unlike for Na, both SCMs greatly reduced the concentration of K in the pore solution, from around 400 to 300 mmol/L (see Table 12).

The decreased amount of K in the pore solution is reflected in the increased amount of K bound by C-A-S-H. PC-L has about 6.9 mmol/100 g cement (32 %), PC-FA has 13.8 mmol/100 g (51 %) and PC-VP has 11.9 mmol/100 g (59 %). The percent of K in non-reactive phases is 14 % for PC-L, the highest of all the cement pastes. PC-FA only has 2 % and PC-VP has 3 % of non-reactive K. The fraction of unreacted K is similar for PC-L and PC-VP (8–9 %), whilst for PC-FA it is 19 %. As with Na, the large difference in distribution is mostly due to the increased alkali metal uptake of C-A-S-H in the cement pastes with SCMs. This reduction in amount and concentration of K in the pore solution is likely the cause of the decreased pH comparing PC-L to PC-FA and VP, going from 13.57 to 13.44.

4.1.6. Impact of temperature on pastes with SCMs

The final effect to consider is how the increased curing temperatures affect cement pastes with SCMs. Table 11 shows that the SCMs only react a few percent more as the temperature is raised from 20 to 38 °C, FA going from 42 to 47 % and VP from 50 to 55 %. The real change occurs at 60 °C, at which point 74 % of FA and 81 % of VP react. This results in the formation of more C-A-S-H, which can be described by the number of moles Si in C-A-S-H (Table 11). Starting with PC-FA, the amount of Si in C-A-S-H increases from 296 to 347 mmol/100 g cement as the temperature increases from 20 to 60 °C. For PC-VP in the same temperature range, the amount of Si increases from 284 to 322 mmol/100 g cement.

Looking first at Na and how its distribution changes, for PC-FA the percent of unreacted Na goes from 18 % at 20 °C to 9 % at 60 °C. This additional 9 % reactive Na appears to distribute evenly between the pore solution and C-A-S-H, as both fractions increase by around 4 to 5 %. For PC-VP, the increased reaction changes the fraction of unreacted Na from 15 to 7 %. However, the Na does not distribute evenly among C-A-S-H and the pore solution as in PC-FA. Instead, the fraction of Na in C-A-S-H decreases from 41 to 38 %, and the fraction in the pore solution increases from 23 to 33 %. This is reflected in the measured concentration of Na. PC-VP at 60 °C has a Na concentration of 276 ± 5 mmol/L, which is higher than even the PC paste at maximum 260 ± 3 mmol/L.

The fraction of unreacted K in PC-FA changes similarly to the fraction of Na. Elevating the curing temperature from 20 to 60 °C reduces the fraction of unreacted K from 19 to 7 %. The extra K does however not distribute in the same way as Na. Of the additional 11 % K that reacts, 8 % goes to C-A-S-H and only 3 % goes into the pore solution. This is reflected in the concentration of K, which is similar for PC-FA at 20 and 60 °C.

The change in K distribution for PC-VP is very small, with only a 1 % decrease in the fraction of unreacted K as the temperature increase from 20 to 60 °C (from 8 to 7 %). For the same temperature change, the C-A-S-H fraction decreases from 59 to 55 %, and the pore solution fraction increases from 31 to 35 %.

As with the PC and PC-L pastes, the pH in PC-FA and PC-VP decreases with increasing temperature. PC-FA goes from a pH of 13.44 to 13.29, and PC-VP from 13.44 to 13.25. This is again despite increasing concentrations of Na and K, especially for VP, and again can be explained by the large increase in sulphate concentration.

The results here highlight that pH is influenced by temperature, both in neat PC and in PC with limestone or SCM replacements. However, it is arguable that pH is a bad measurement of pore solutions in the way it is measured here. The pH of water is inherently influenced by temperature. As the temperature increases, the pH decreases. For cement pore solutions such as those in this study a decrease from 13.6 to 12.4 is expected as the measurement temperature increases from 20 to 60 °C. An example of this in "Appendix D: Influence of temperature on pore solution pH". This temperature induced change is around five times larger than the difference in pH between for instance PC and PC-VP at 20 °C.

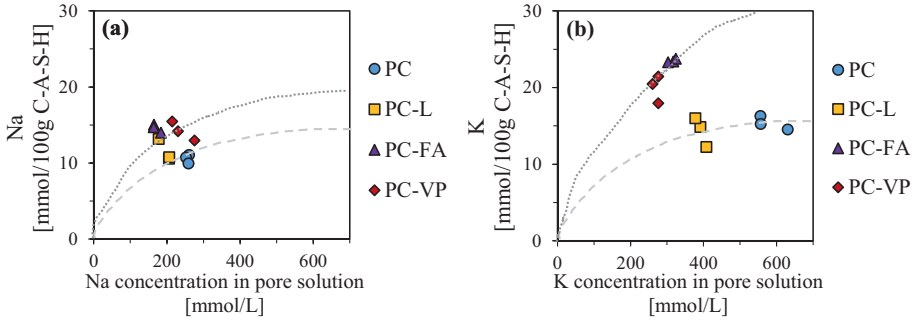

Fig. 15. Change in the amount of Na (a) and K (b) in C-A-S-H as it varies with the concentration in the pore solution, normalized to the amount of C-A-S-H. The dashed and dotted lines in the plots are only included as guides for the eye and show one possible type of adsorption isotherm. The dashed line represents hypothesized change for dilution of PC with limestone, and the dotted line represents replacement of PC with pozzolanic SCMs. More data points at different concentrations are needed to establish the true adsorption isotherms.

4.2. Important factors for alkali metal distribution

In the previous section we have seen how Na and K are distributed between the pore solution, C-A-S-H, non-reactive phases, and unreacted phases. Now we examine why they distribute in this way. We can consider the hydrated paste system as one where if there was no C-A-S-H, all Na and K would be distributed between the non-reactive phases, unreacted phases, and the pore solution. C-A-S-H therefore is the main controlling factor of the final distribution, and it all hinges on its properties and ability to bind Na and K. Several factors that influence alkali metal ion uptake by C-A-S-H have been proposed, such as pore solution concentration [79] and Ca/Si ratio [8–10].

Fig. 15 shows how the amount of Na and K in C-A-S-H change with the concentrations of Na and K in the pore solution. Here the amount is normalized to 100 g C-A-S-H to highlight the difference between the nature of C-A-S-H in the different pastes. Although the effect is more subtle for Na than for K, there appears to be a pattern. The included dashed and dotted lines in the figure are drawn as guides for the eye and resemble binding isotherms, analogous to our previous publications on chloride binding (a recent example can be found in [74]). Bear in mind that the included isotherms in Fig. 15 are only hypothetical, as more data points at different concentrations are needed to establish the true adsorption isotherm. The included isotherms are similar to the relationship between K/Si and concentration of K reported by Hong and Glasser [26]. Considering Fig. 15 it appears as though PC and PC-L follow the same binding isotherm, whilst PC-VP and PC-FA follow another. This demonstrates how pozzolanic SCMs truly alter the nature of C-A-S-H in ways that promote sorption of Na and K. It also means that whilst alkali metal binding is influenced by pore solution concentrations, it is not the only factor.

Fig. 16 shows how the Na/Si and K/Si ratio of the C-A-S-H change with Ca/Si and Al/Si (Table 10). The trends here are less pronounced for Na than for K, and the low Ca/Si of PC-L at 60 °C also distracts from the trends. We can however see indications of increasing (Na,K)/Si with decreasing Ca/Si and with increasing Al/Si. This supports the idea that having less Ca and/or more Al in the C-A-S-H makes its surface more negatively charged, thereby adsorbing more alkali metal cations [25,26]. Our values for Ca/Si and Al/Ca in PC-FA are similar to those of Duchesne and Bérubé [47], who reported Ca/Si between 1.35 and 1.44 and Al/Ca from 0.12 to 0.13 for their fly ash pastes with 40 % replacement.

Our findings thus generally agree with the literature, but the inclusion of C-A-S-H quantification from the mass balance provides an additional insight. Although studies have reported the relationship between C-A-S-H composition and alkali metal binding [8–10], they report the increased (Na,K)/Si ratios without considering the change in amount of C-A-S-H formed in real cement pastes with SCMs. Table 11 shows that at 20 and 38 °C there is less total C-A-S-H formed in the PC-FA and PC-VP pastes than in PC. We can therefore conclude that the ASR mitigating effects of these SCMs is caused by changes in the C-A-S-H composition, not because they produce additional C-A-S-H through the pozzolanic reaction.

We wish to briefly highlight the observed differences between Na and K in the cement pastes. The results of the present study find that a larger fraction of the Na is bound by C-A-S-H than K, but that since there is much more K in all the pastes the amount of K in C-A-S-H is larger.

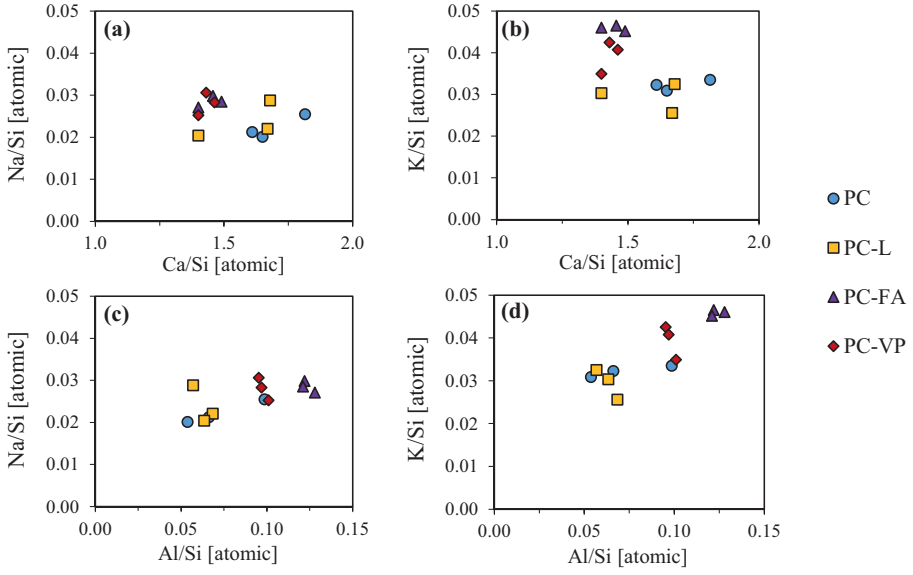

Fig. 16. Change in composition of C-A-S-H: Na/Si (left) and K/Si (right) with change in Ca/Si (a, b) or Al/Si (c, d).

There has been active debate on whether or not Na and K are preferentially adsorbed on C-A-S-H. Some studies conclude that they are adsorbed equally [8,26], whilst other report that one or the other is favoured [54,80]. Our results are not conclusive regarding this question, as Na appears to be preferentially taken up by C-A-S-H in the PC, PC-L, and PC-FA pastes but not in PC-VP. The difference between Na and K was also pointed out by Taylor [54]. This highlights the importance of reporting both Na and K separately in ASR studies.

4.3. Relation to accelerated testing of ASR expansion

This study is focused on the chemistry of cement paste and can not necessarily be applied directly to paste as it exists in concrete. There is still the missing link of how aggregates influence the alkali metal distribution, both in terms of supplying, adsorbing, and creating sinks through the formation of alkali silica gel. This is still an unresolved question [4,46,53,81]. However, the results of this study can give insight into how the paste in concrete might behave in a manner independent of which aggregate is used. We now have data on the behaviour of the pore solution and C-A-S-H, and the pore solution is key in the dissolution of silicates in aggregates, which is the starting point for ASR.

Let us now consider how the observed temperature effects on alkali metal distribution might be reflected in concrete expansion. Starting at the reference temperature of 20 °C, we unfortunately do not have expansion data yet due to the slow rate of reaction at realistic temperatures. Patient readers are encouraged to look for these expansion values once the NEWSCEM field station testing concludes in a decade or two. Despite the current lack of expansion data, we can still hypothesize about the effect of the SCMs. As discussed in Section 4.1.5, both SCMs reduce the concentrations and amounts of Na and K in the pore solution, thereby also reducing the pH. Lowering the pH reduces the dissolution rate of silicates, which is considered the rate determining step of ASR.

The general trend of all the results in this study is that there are only small differences between the same paste at 20 and 38 °C curing temperature. All trends in the differences between PC, PC-L, PC-FA, and PC-VP are also similar at 20 and 38 °C. There are some minor differences, such as higher contents of bound water at 20 °C, but in general the two curing temperatures result in similar cement pastes. This makes a good case for the viability of accelerated tests performed at 38 °C.

This is however not the case for curing at 60 °C. There are quite extreme differences in the cement pastes at 20 and 60 °C, both in terms of the pore solution and the hydrated phases. In the pore solution we see a near tenfold increase in the concentration of sulphate [31], which acts to lower the concentration of OH^- if the Na^+ and K^+ concentrations remain constant. This compounds with the inherent lowering of pH at elevated temperatures, further differentiating the paste systems at these two temperatures. We have also seen the trend of a larger share of alkali metals being available in the pore solution at 60 °C, thereby unrealistically accelerating ASR.

In the hydrates, the composition of C-A-S-H and its behaviour also changes greatly. The wide spread of Ca/Si-values in Fig. 8 could indicate that different types of C-A-S-H are formed in different locations, making the paste more heterogeneous. Most concerning is perhaps the PC-L paste, which exhibits unrealistically low Ca/Si in its C-A-S-H despite providing little extra Si to the cement. If the characterization performed in this study holds true, it means that even a supposedly inert filler can alter the main hydrate phase in an extreme manner at high curing temperatures. We also see the signs of extremely accelerated reaction of the SCMs (Table 11), increasing with 30 % > from 20 to 60 °C. The increased amount of C-A-S-H formed (also Table 11) as a result further separates the accelerated testing at 60 °C from cement and concrete cured in realistic temperatures. From the perspective of cement paste chemistry, this high curing temperature essentially creates a different chemical system than curing at 20 °C.

Several researchers have compared the expansion of the mortar or concrete prisms, and the pore solution of the respective cement pastes [14,15,47]. Fig. 17 shows for our data the expansion of the concrete prisms at 90 and 180 days curing compared to both the concentration of OH^- ((a), also see Fig. 7) and to the sum of the concentrations of Na and K (b). Expansion data and pore solution for 90 days can be found in the supplementary data of this paper. As the other researchers, we observed a lower boundary of (Na + K) concentration, i.e. approx. 0.5 mol/L, below which expansion is likely to be reduced below critical limits (e.g., 0.03 % expansion at 1 year as used in [65,66]). The effect of temperature on expansion can be seen in Fig. 17(a). Bear in mind that the lines in Fig. 17(a) are just intended as guides for the eye, as the relationship between expansion and alkali metal concentration is not linear due to the pessimum effect [82]. The increased concentration of sulphate reduces the OH^- concentration when going from 38 to 60 °C, but the elevated temperature also accelerates ASR. For this mix of aggregates, there appears to be a correlation between OH^- concentration and expansion, but both the slope and intercept of the line is affected by the curing temperature. The intercept is about 0.25 mol/L for 60 °C and 0.4 mol/L for 38 °C.

4.4. Predicting ASR mitigating properties of new SCMs

We wish now to summarize how we believe the alkali metal distribution relates to ASR, in a way that is useful for engineers. Fig. 18 shows how the mass percentages of Na_2O and K_2O are distributed between what is available for ASR and what is not. We consider the Na and K in the pore solution to be available, whilst those in non-reactive and unreacted phases or bound by C-A-S-H are unavailable. A calculated Na_2O_{eq} is also included, though we wish to reiterate that it is a poor measure that completely obfuscates the differences between Na and K. This study demonstrates that these two elements are not equivalent, and we strongly encourage all future researchers to report Na and K separately.

The main takeaway from Fig. 18 is that only around 40 % of Na_2O and 50 % of K_2O are likely to contribute to ASR in concrete with PC or PC with partial limestone replacement. This is similar to the numbers found for OPC by Duchesne and Bérubé [47], who suggested around 50 % of

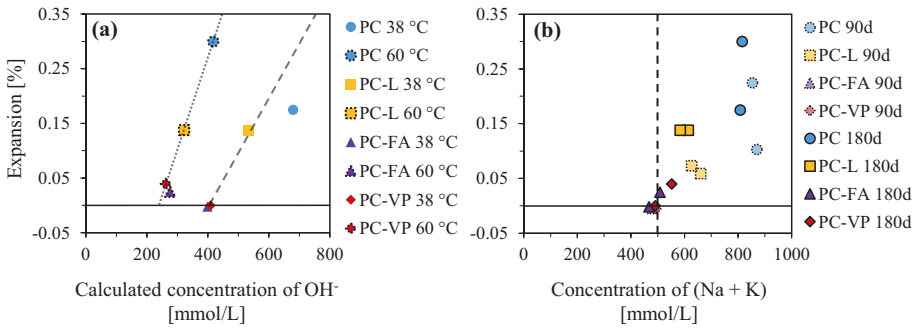

Fig. 17. Expansion of concrete prisms made with the four cements in this project, cured at both 38 and 60 °C. The pore solution data is from cement pastes cured for 90 and 180 days, whereas the expansion is from concretes cured for 13 weeks (60 °C), 16 weeks (38 °C) and 26 weeks (38 and 60 °C). Subfigure (a) shows expansion at 180 days as it varies with the concentration of OH^-, which was calculated based on the composition of the pore solution. Lines are included to show the general trend of expansion with concentration at 38 °C (dotted) and 60 °C (dashed). Subfigure (b) shows the expansion as it varies with the sum of the concentrations of Na and K. A dashed line is included to indicate the (Na + K) concentration below which we expect below critical expansion.

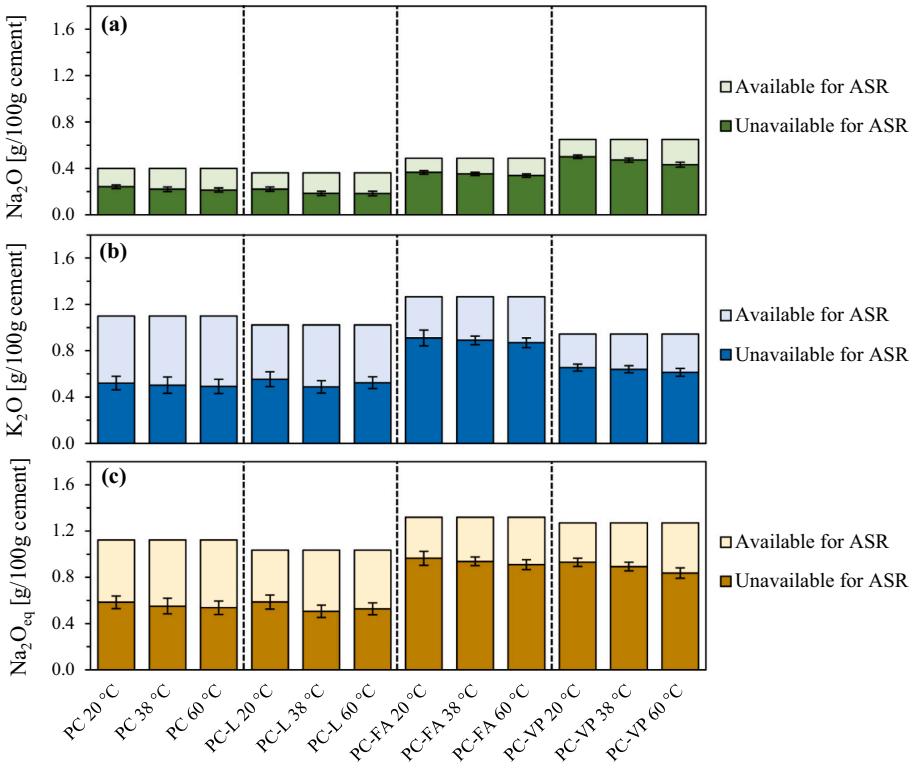

Fig. 18. Masses of Na_2O (a) and K_2O (b) in the different cements as they distribute between what is available for ASR and what is not. Na and K in the pore solution are considered available, whilst those bound by C-A-S-H and in unreacted phases are not. A calculated Na_2O_{eq} is also included (c). The black error bars are from Gaussian error propagation of the bound water content determined with TGA (10 %), and the standard deviation of ICP-OES measurements.

Na_2O_{eq} to be available for reaction. For cements with SCMs a much lower amount of alkali metals are available. Only around 20–30 % of Na_2O and K_2O in PC-FA and PC-VP are available for ASR, in the same range of 15–30 % of Na_2O_{eq} reported previously [47]. This result should influence how the "alkali loading" of cements are interpreted, for instance in ASR models.

We have demonstrated in this study that VP appears to work similarly to FA in mitigating ASR expansion, although it is slightly less effective. However, this can not necessarily be extrapolated to be true for natural pozzolans in general. Natural pozzolans vary in chemical and mineralogical composition, and in various physical properties. The VP we have investigated is of a particular fineness, morphology, chemical and mineral composition, all of which influence how it behaves in the cement paste. It is important for selections of new SCMs to understand which of these factors determine the SCMs impact on durability.

Based on the findings of this study we can make some suggestions of important factors for new SCMs, and some methods that might give indications of its performance. As literature has shown it is beneficial that SCMs have high contents of Si and Al [8,10,20,26]. These elements should ideally be in reactive phases with sufficiently small particle sizes so that they react quickly and can contribute to form C-A-S-H. We have however shown that the actual "alkali content" of an SCM is far from the only important factor when considering how the SCM contributes with alkali metals to the system. Some materials have significant portions of its alkali metals incorporated in stable crystalline phases that are unlikely to react [33]. The physical properties such as fineness are also important, as more finely ground materials will react more readily and can therefore be better at mitigating ASR [11,34]. These findings highlight the importance of not only relying on XRF for screening new materials, but also to perform QXRD analysis to determine the crystalline phases. Combining this with a technique like SEM-EDS will also enable distinguishing between different types of similar minerals where the XRD might be unable to distinguish solid solutions.

When it comes to methods for testing the paste, it seems like the concentrations of Na and K alone can give reasonable estimates for the starting point of expansion. Rather than prescribing a mass of "Na_2O_{eq}" for a given reactive mix of aggregates, we could focus on the pore solution of the cement paste. The cement could be tuned so that the pore solution in the paste only has a certain concentration of (Na + K), below which we avoid expansion. This general idea should hold for cements both with and without SCMs, removing the need for separate criteria for PC and composite cements [40]. Once a reasonable lower limit has been determined, a new cement mixture could then be evaluated by measuring the pore solution with ICP or a flame spectrophotometer. If future studies on cold water extraction [83] of pore solution prove it to be reliable at extracting Na and K, we can even skip the dangerous pore solution expression. TGA analysis could then be used to get the amount of free water in the paste. Using this volume and the concentrations, we can immediately get a similar idea of the alkali metal distribution like those presented in Fig. 18.

4.5. Limitations and further research

Having discussed the results and their implications, a critical look at the limitations of our approach is in order. In this work we have presented a methodology for determining the distribution of alkali metals in hydrated cement pastes and linking it to ASR expansion. There is room for improvements in several of the methods that were used.

In this study we used a 22 % replacement of clinker for our cements, with 18 % of the pozzolanic SCMs. This is a realistic level of replacement used in Norwegian cements, so the results of this study should apply well to similar industrial cements. However, the relatively low replacement level limits the impact of the SCMs and makes it harder to distinguish between them. Thus, further work in this field should use higher levels of replacement, which matches the future trend for blended cements used in practice. It might also be of interest to re-evaluate the dilution

effect of limestone by using a pure $CaCO_3$ filler rather than an industrial limestone that contains Na and K.

Characterizing C-A-S-H is perhaps the most pivotal point in any cement paste mass balance. Since it is the most abundant phase by a large margin, any error in characterization has large effects on all following calculations. We have seen here that there are several issues with traditional SEM-EDS characterization. Detection of Na and K is difficult, either because too little was detected, or as for PC-FA and PC-VP at 60 °C where too much was detected. There is a risk that sample preparation leads to precipitation on the cut sample surface [47]. Determining the Ca/Si ratio also appears to be highly unreliable, even for simple substitution of PC with limestone filler. Our mass balance had to use a lower limit for Ca/Si at 1.4, which we deemed realistic due to all pastes having significant CH content. Any lower value would invalidate the calculations, which shows that there is a discrepancy between results from SEM-EDS and the other inputs to the mass balance. We recommend that future researchers attempt to incorporate C-A-S-H characterization with NMR or EDS hypermaps [84,85] as a way of checking the observations in SEM-EDS. There are also many settings and parameters in the SEM-EDS that could be tuned, such as dwell time, accelerating voltage, and current. Due to the simplicity and availability of this technique, any research into optimal parameters for C-A-S-H characterization that includes Na and K would be highly desired.

The mass balance calculations are performed in many steps, which means the experimental error propagates and compounds. Beyond the uncertainty propagation, there are some ways future mass balances could be improved. The present model assumes that all Mg forms periclase. This was chosen since neat clusters of Mg with only minor amounts of other elements are often observed in SEM-EDS maps of Norwegian cements. Other cements might form hydrotalcite instead, which is thermodynamically favoured in many cases. The present mass balance also forms both monosulphate and monocarbonate AFm phases simultaneously, although thermodynamically only one will be stable at a time [86]. In the XRD spectra we can however observe both carbonate and sulphate AFm, likely because the systems are not at equilibrium (see "Appendix C: X-ray diffraction spectra"). Whether to include both phases at the same time should be reconsidered. It could also be prudent to include hemicarbonate AFm and consider its solid solution with monosulphate AFm [87].

The calculated degree of reaction from the mass balance might be overestimated, especially at 60 °C. Our best confirmation is visual, as there is a very clear difference in the microstructure in the pastes at 60 °C compared to those at 20 and 38 °C. At 60 °C we struggle to locate unreacted particles of FA and VP, and the only ones we clearly see are quite large. It is likely that most of the smallest and medium sized reactive particles have already reacted, leaving only the largest particles and those that are non-reactive. We would recommend including SEM image analysis or some other supplementary methods to quantify SCM reaction.

Since this study focuses on cement paste, we must exercise caution in applying the results to concrete. The aggregates might release Na and K, some might adsorb on the surface, and the ASR gel will consume alkali metals. We encourage attempts to make alkali metal balances for the more complex concrete system and hope that our work here can help these endeavours.

5. Conclusion

The distribution of alkali metals is important to understand how SCMs and curing temperature affect the alkali metals in pore solution contributing to ASR. This paper presents a methodology for investigating how the alkali metals distribute between non-reactive phases, unreacted phases, C-A-S-H, and pore solution in hydrated cement pastes. We have documented the complete cement paste systems, including hydrate assemblage, pore solution, and concrete expansion. We have investigated the effect of clinker replacement by 22 % with limestone, fly ash (FA) and a volcanic pozzolan (VP), as well as the effect of elevating curing temperature from 20 to 38 and 60 °C. With the inclusion of limestone references we are able to distinguish the effects of PC dilution and the pozzolanic reaction of the SCMs.

Building on the work of Duchesne and Bérubé [47] we have expanded the number of parameters to include filler dilution and curing temperature, and experimentally investigated various assumptions regarding the alkali metal distribution. Our findings verify some of the previously reported calculations for PC and PC-FA cured at 38 °C.

The alkali distribution for the PC and PC-L reference pastes at 20 °C show that less than half of the Na and K are found in the pore solution, whereas the about half is associated with C-A-S-H, and less than 10 % is found in unreacted clinker phases. Partial replacement of PC with limestone lead to a decrease in total Na and K content, with more K bound in the non-reactive phases in the limestone. Limestone replacement led to a reduction in alkali metal concentrations roughly proportional to its replacement level but did not greatly reduce the fraction of Na and K in the pore solution.

At 20 °C the inclusion of FA and VP lead to a large increase in total alkali metal content for the paste, yet they reduced the fraction of Na and K in the pore solution. This was mostly caused by increased alkali metal uptake by C-A-S-H, but also due to the larger amounts of Na and K bound in non-reactive and unreacted phases. Particularly for VP we found that 40 % of its 1.7 wt% Na_2O were bound in the non-reactive minerals such as aegirine and andesine. This highlights that it is vital for the use of new SCMs to characterize their crystalline, non-reactive phases. Another important observation is that the pastes with pozzolans had more C-A-S-H than in the limestone paste, but less C-A-S-H than the pure PC paste at 20 and 38 °C.

Elevating the curing temperature from 20 to 38 °C had little effect on concentrations of elements and on the distribution of Na and K. In PC there was a small trend of Na moving from C-A-S-H to pore solution at higher temperatures, whilst no similar trend was found for K. At 60 °C a variety of factors changed to make the system completely different than pastes cured at 20 or 38 °C. The degree of reaction for FA and VP increased by 30 %, resulting in an increase in the amount of C-A-S-H formed. The concentration of sulphate in the pore solution increased greatly, resulting in lower pH and OH^- concentration.

Relating the cement pastes to the expansion of concrete prisms cured at 38 and 60 °C there appears to be a (Na + K) concentration around 0.5 mol/L below which there is no critical expansion. Studying the pore solution of cement pastes with new SCMs appears to be a good test for screening their durability impact with respect to ASR.

CRediT authorship contribution statement

Petter Hemstad: Conceptualization, methodology, software, formal analysis, investigation, verification, visualization, writing – original draft, writing – review & editing.
Pamela Zuschlag: Investigation, methodology.
Petter Kjellemyr: Investigation.
Jan Lindgård: Investigation, supervision, writing – review & editing.
Knut O. Kjellsen: Resources, supervision.
Terje F. Rønning: Resources, supervision.
Harald Justnes: Supervision.
Maciej Zajac: Resources, investigation.
Mohsen Ben Haha: Resources, funding acquisition.
Klaartje De Weerdt: Supervision, methodology, project administration, conceptualization, funding acquisition, writing – review & editing.

Declaration of competing interest

The authors declare the following financial interests/personal relationships which may be considered as potential competing interests:
Knut Kjellsen, Terje Rønning, Maciej Zajac, and Mohsen Ben Haha are currently employed at Heidelberg Materials. Heidelberg are

intending to produce cement with the volcanic pozzolan provided for this study.

Most of this study was performed independently by Petter Hemstad, who was salaried by NTNU during the project and received funding for the experimental work from among another Heidelberg.

Petter Hemstad will start working for Heidelberg Materials from the 1st of August 2023.

Data availability

Data will be made available on request.

Acknowledgements

The authors would like to thank Ingrid Masdal for her assistance with sample preparation and analysis, and Steinar Seehus for assistance with pore solution expression. Thank you to Heidelberg Materials Global R&D for providing characterization of the raw materials. Thanks to Tobias Danner (SINTEF) for performing Rietveld refinement of the XRD scans and providing thorough descriptions of the aggregates and Rietveld methodology. Thank you to Mikael Dissing at DTI for preparing the SEM polished sections. Thanks to Barbara Lothenbach, Mahsa Bagheri, and Børge Johannes Wigum for helpful discussions. We also wish to thank Syverin Lierhagen, Anica Simic, Kyyas Seyitmuhammedov (NTNU), Bjarne Nenseter (SINTEF) and Bin Ma (EMPA) for performing ICP analyses. Thank you to all the participants in the NEWSCEM project. Finally, a thank you to Ola Skjølsvold and the team at SINTEF for the casting and performance testing of the concrete specimen.

Funding

This work was supported by NTNU through salary for Petter Hemstad; the Norwegian Research Council, Heidelberg Materials Sement Norge AS, Norbetong, Mapei, Rambøll, Skanska, Spenncon, IBRI Rheocenter, the Norwegian Public Roads Administration, and NTNU, through the NEWSCEM project (Norwegian Research Council project number 282578).

Appendix A. Pore solution analysis results table

Table 12
Results of ICP-OES/MS and pH measurements of the cement paste pore solutions, expressed after 180 days curing. The error included is the standard deviation of three parallel samples.

Cement	Temp.	Al	Ca	K	Na	S	Si	pH
	[°C]	[mmol/L]	[mmol/L]	[mmol/L]	[mmol/L]	[mmol/L]	[mmol/L]	[−]
PC	20	0.43 ± 0.01	1.72 ± 0.06	631 ± 8	260 ± 3	19.1 ± 0.8	0.44 ± 0.04	13.63 ± 0.02
	38	0.16 ± 0.01	1.77 ± 0.06	556 ± 34	252 ± 14	62.1 ± 0.6	0.29 ± 0.01	13.57 ± 0.14
	60	0.19 ± 0.01	3.0 ± 0.2	557 ± 8	259 ± 3	195 ± 3	0.26 ± 0.05	13.43 ± 0.02
PC-L	20	0.17 ± 0.01	1.78 ± 0.04	392 ± 36	178 ± 16	15.5 ± 0.5	0.24 ± 0.01	13.57 ± 0.02
	38	0.09 ± 0.01	1.78 ± 0.03	408 ± 5	206 ± 3	37.6 ± 0.8	0.24 ± 0.04	13.56 ± 0.04
	60	0.17 ± 0.01	2.77 ± 0.01	378 ± 5	206 ± 4	128 ± 3	0.26 ± 0.01	13.33 ± 0.01
PC-FA	20	1.0 ± 0.3	1.6 ± 0.7	317 ± 52	165 ± 13	12.3 ± 0.8	0.81 ± 0.12	13.44 ± 0.01
	38	0.59 ± 0.03	0.9 ± 0.1	303 ± 2	164 ± 2	31.2 ± 0.5	0.90 ± 0.02	13.42 ± 0.06
	60	0.40 ± 0.02	1.82 ± 0.08	324 ± 10	184 ± 4	113 ± 2	0.55 ± 0.03	13.29 ± 0.01
PC-VP	20	0.56 ± 0.01	1.1 ± 0.2	277 ± 7	215 ± 6	11.1 ± 0.7	0.54 ± 0.01	13.44 ± 0.01
	38	0.48 ± 0.03	1.09 ± 0.05	261 + 2	230 ± 2	38.1 ± 3.5	0.54 ± 0.04	13.37 ± 0.01
	60	0.27 ± 0.02	2.4 ± 0.14	277 ± 9	276 ± 5	142 ± 4	0.42 ± 0.04	13.25 ± 0.01

Appendix B. Thermogravimetric analysis results

These TGA curves all include the mass loss (TG, top) and derivative of mass loss (DTG, bottom) from 40 to 900 °C.

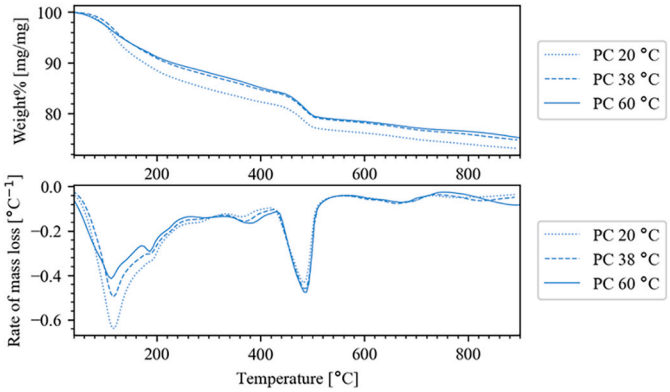

Fig. 19. Mass loss (top) and derivative of mass loss (bottom) for the PC pastes at 180 days.

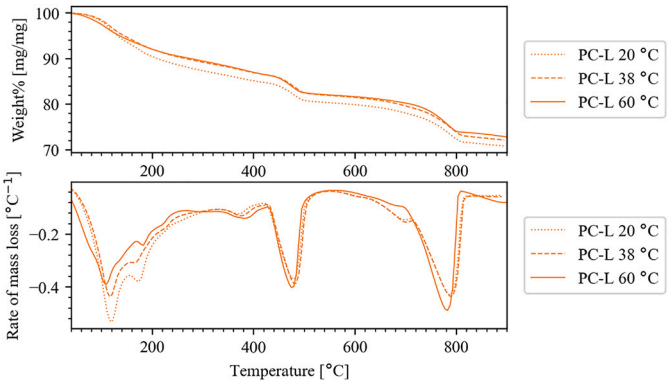

Fig. 20. Mass loss (top) and derivative of mass loss (bottom) for the PC-L pastes at 180 days.

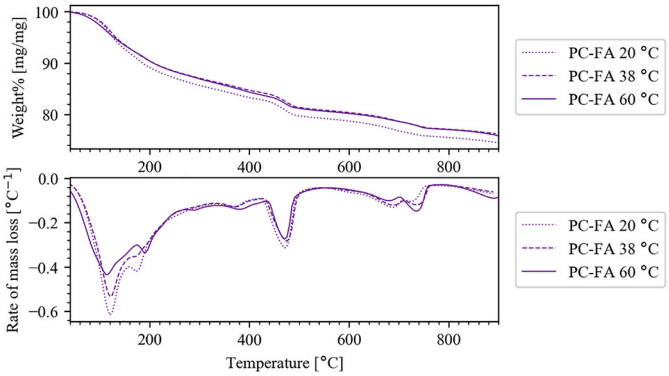

Fig. 21. Mass loss (top) and derivative of mass loss (bottom) for the PC-FA pastes at 180 days.

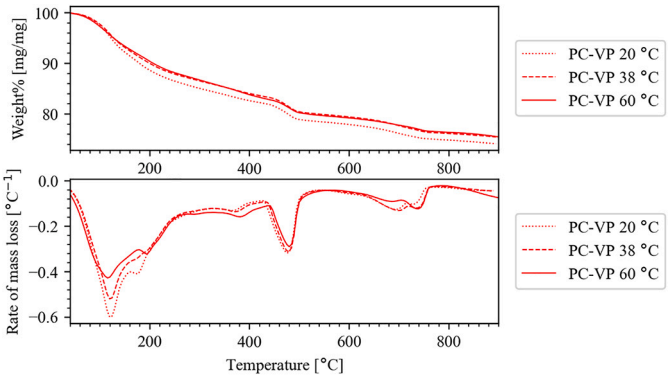

Fig. 22. Mass loss (top) and derivative of mass loss (bottom) for the PC-VP pastes at 180 days.

Appendix C. X-ray diffraction spectra

This appendix includes figures for the XRD scans of the hydrated cement pastes. They are organized with one cement and three curing temperatures per figure. Only small angles 8-14 2θ are included, as the main phases of interest have characteristic peaks in this region.

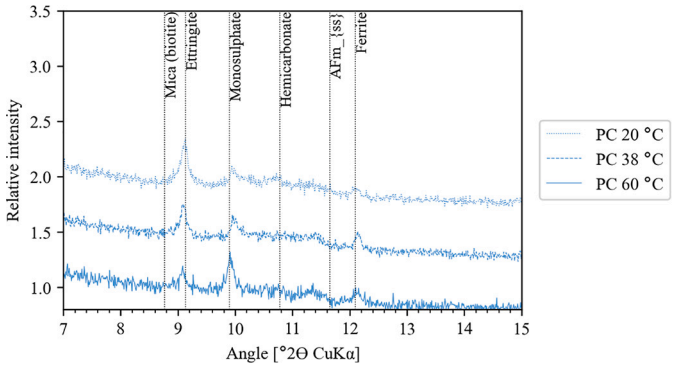

Fig. 23. Low angle XRD spectra for the PC pastes at 20, 38, and 60 °C curing temperatures.

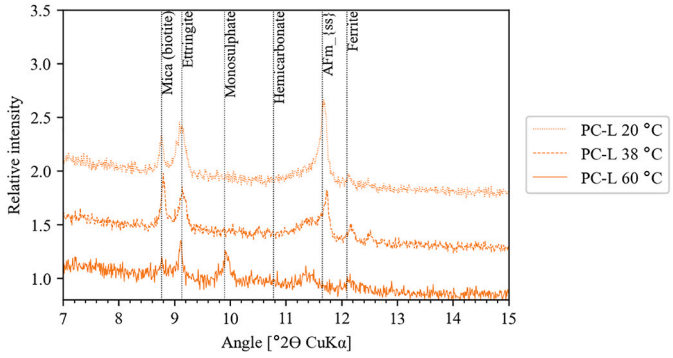

Fig. 24. Low angle XRD spectra for the PC-L pastes at 20, 38, and 60 °C curing temperatures. The large biotite peak is likely caused by preferential orientation, since the 20 and 38 °C pastes were front loaded into the XRD sample holders.

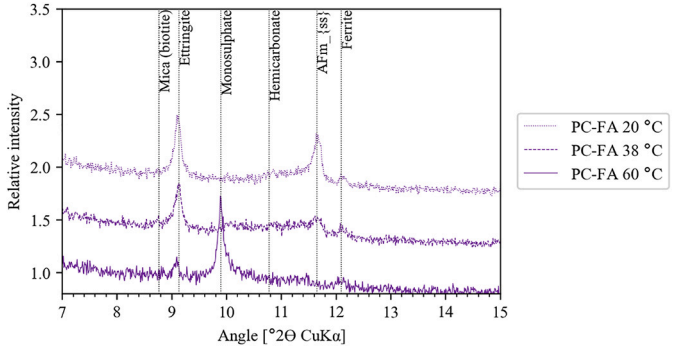

Fig. 25. Low angle XRD spectra for the PC-FA pastes at 20, 38, and 60 °C curing temperatures.

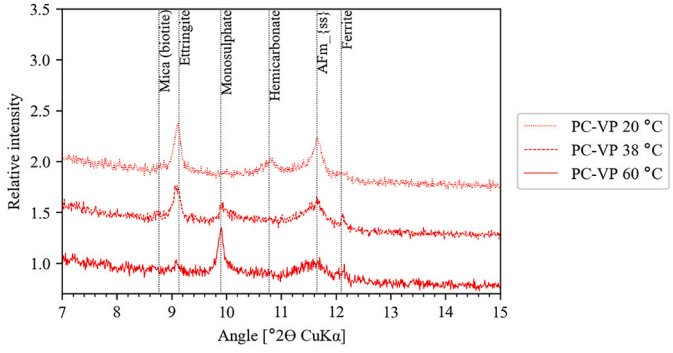

Fig. 26. Low angle XRD spectra for the PC-VP pastes at 20, 38, and 60 °C curing temperatures.

Appendix D. Influence of temperature on pore solution pH

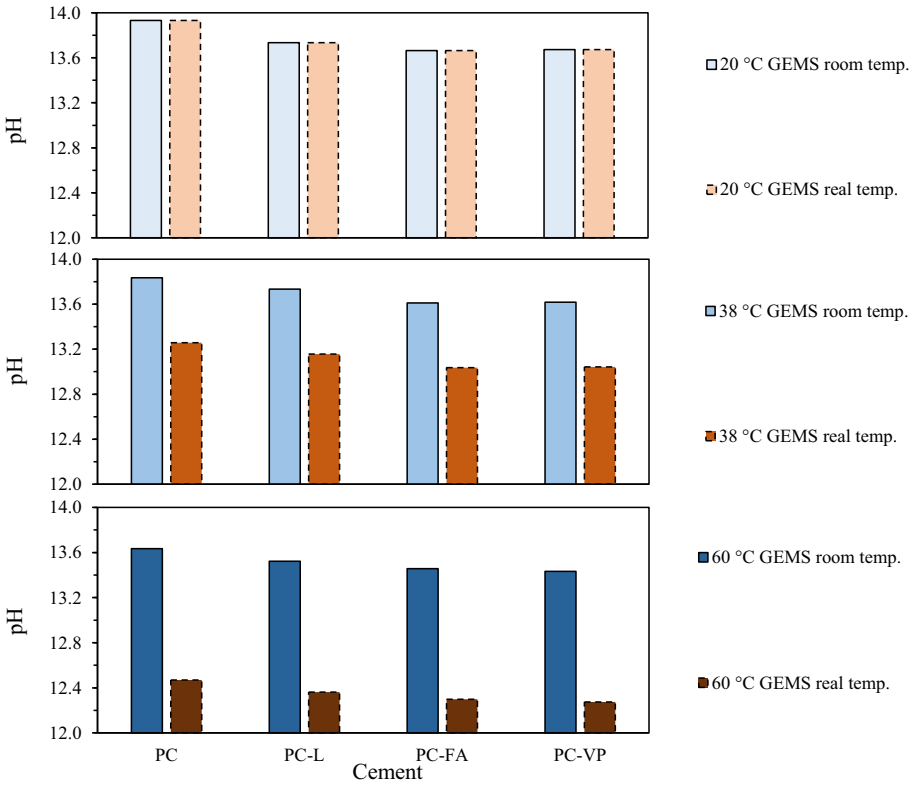

Fig. 27. Illustration of how temperature influences pH in cement paste pore solutions. The temperature (20, 38, and 60 °C) refers to the curing temperature of each paste. The pore solution data from this study was put into a thermodynamic model in GEMS, and the pH was calculated for two different conditions: For the solution at room temperature ("GEMS room temp"), and for the solution at its real curing temperature ("GEMS real temp."). At 38 and 60 °C the effect of temperature on pH is much larger than any difference caused by PC replacement with limestone, FA, or VP.

References

[1] I. Sims, A. Poole (Eds.), Alkali-Aggregate Reaction in Concrete: A World Review, 2017.

[2] J. Custódio, J. Lindgård, B. Fournier, A. Santos Silva, M.D.A. Thomas, T. Drimalas, J.H. Ideker, R.-P. Martin, I. Borchers, B. Johannes Wigum, T.F. Rønning, Correlating field and laboratory investigations for preventing ASR in concrete – the LNEC cube study (part I – project plan and laboratory results), Constr. Build. Mater. 343 (2022), 128131.

[3] S.S. Kongshaug, R.M. Larssen, M.A.N. Hendriks, T. Kanstad, G. Markeset, Load effects in reinforced concrete beam bridges affected by alkali–silica reaction—constitutive modelling including expansion, cracking, creep and crushing, Eng. Struct. 245 (2021).

[4] C. Drolet, J. Duchesne, B. Fournier, Effect of alkali release by aggregates on alkali-silica reaction, Constr. Build. Mater. 157 (2017) 263–276.

[5] M.A. Bérubé, J.F. Dorion, J. Duchesne, B. Fournier, D. Vézina, Laboratory and field investigations of the influence of sodium chloride on alkali–silica reactivity, Cem. Concr. Res. 33 (2003) 77–84.

[6] H.F.W. Taylor, Cement Chemistry, Thomas Telford, 1997.

[7] M. Shehata, M.D.A. Thomas, Alkali release characteristics of blended cements, Cem. Concr. Res. 36 (2006) 1166–1175.

[8] E. L'Hôpital, B. Lothenbach, K.L. Scrivener, D.A. Kulik, Alkali uptake in calcium alumina silicate hydrate (C-A-S-H), Cem. Concr. Res. 85 (2016) 122–136.

[9] Y. Yan, S.-Y. Yang, G.D. Miron, I.E. Collings, E. L'Hôpital, J. Skibsted, F. Winnefeld, K.L. Scrivener, B. Lothenbach, Effect of alkali hydroxide on calcium silicate hydrate (C-S-H), Cem. Concr. Res. 151 (2022), 106636.

[10] T. Chappex, K.L. Scrivener, Alkali fixation of C–S–H in blended cement pastes and its relation to alkali silica reaction, Cem. Concr. Res. 42 (2012) 1049–1054.

[11] R.D. Kalina, S. Al-Shmaisani, S. Seraj, R. Cano, R.D. Ferron, M.C.G. Juenger, Role of alkalis in natural pozzolans on alkali-silica reaction, MJ 118 (2021).

[12] M. Bagheri, B. Lothenbach, M. Shakoorioskooie, K.L. Scrivener, Effect of different ions on dissolution rates of silica and feldspars at high pH, Cem. Concr. Res. 152 (2022), 106644.

[13] M. Shehata, M.D.A. Thomas, Use of ternary blends containing silica fume and fly ash to suppress expansion due to alkali–silica reaction in concrete, Cem. Concr. Res. 32 (2002) 341–349.

[14] M. Shehata, M.D.A. Thomas, R. Bleszynski, The effects of fly ash composition on the chemistry of pore solution in hydrated cement pastes, Cem. Concr. Res. 29 (1999).

[15] M. Bagheri, B. Lothenbach, K.L. Scrivener, The effect of paste composition, aggregate mineralogy and temperature on the pore solution composition and the extent of ASR expansion, Mater. Struct. 55 (2022) 192.

[16] J. Duchesne, M.A. Bérubé, The effectiveness of supplementary cementitious materials in suppressing expansion due to ASR: another look at the reaction mechanisms. Part 2: pore solution chemistry, Cem. Concr. Res. 24 (1994).

[17] J.J. Kollek, S.P. Varma, C. Zaris, Measurement of OH- concentrations of pore fluids and expansion due to alkali-silica reaction in composite cement mortars, in: Proc. 8th Int. Congress on the Chemistry of Cement 3, 1986, pp. 183–189.

[18] M. Kawamura, K. Takemoto, Correlation between pore solution composition and alkali silica expansion in mortars containing various fly ashes and blastfurnace slags, Int. J. Cem. Compos. Light. Concr. 10 (1988).

[19] M.D.A. Thomas, D. Hooton, K. Folliard, Prevention of alkali-silica reaction, in: I. Sims, A. Poole (Eds.), Alkali-Aggregate Reaction in Concrete: A World Review, 2017, pp. 89–118.

[20] S.M.H. Shafaatian, A. Akhavan, H. Maraghechi, F. Rajabipour, How does fly ash mitigate alkali–silica reaction (ASR) in accelerated mortar bar test (ASTM C1567)? Cem. Concr. Compos. 37 (2013) 143–153.

[21] I. Canham, C.L. Page, P.J. Nixon, Aspects of the pore solution chemistry of blended cements related to the control of alkali silica reaction, Cem. Concr. Res. 17 (1987).

[22] M. Shehata, M.D.A. Thomas, The role of alkali content of Portland cement on the expansion of concrete prisms containing reactive aggregates and supplementary cementing materials, Cem. Concr. Res. 40 (2010) 569–574.

[23] M.D.A. Thomas, Supplementary Cementing Materials in Concrete, CRC Press, Boca Raton, FL, 2013.

[24] B. Lothenbach, K.L. Scrivener, D. Hooton, Supplementary cementitious materials, Cem. Concr. Res. 41 (2011) 1244–1256.

[25] S.-Y. Hong, F.P. Glasser, Alkali sorption by C-S-H and C-A-S-H gels, Cem. Concr. Res. 32 (2002) 1101–1111.
[26] S.-Y. Hong, F.P. Glasser, Alkali binding in cement pastes part I. The C-S-H phase, Cem. Concr. Res. 29 (1999).
[27] T. Chappex, K.L. Scrivener, The effect of aluminum in solution on the dissolution of amorphous silica and its relation to cementitious systems, J. Am. Ceram. Soc. 17 (2012) n/a-n/a.
[28] M.D.A. Thomas, B. Fournier, K. Folliard, J.H. Ideker, M. Shehata, Test methods for evaluating preventive measures for controlling expansion due to alkali–silica reaction in concrete, Cem. Concr. Res. 36 (2006) 1842–1856.
[29] J. Lindgård, M.D.A. Thomas, E.J. Sellevold, B. Pedersen, Ö. Andiç-Çakır, H. Justnes, T.F. Rønning, Alkali–silica reaction (ASR)—performance testing: influence of specimen pre-treatment, exposure conditions and prism size on alkali leaching and prism expansion, Cem. Concr. Res. 53 (2013) 68–90.
[30] J. Lindgård, Ö. Andiç-Çakır, I. Fernandes, T.F. Rønning, M.D.A. Thomas, Alkali–silica reactions (ASR): literature review on parameters influencing laboratory performance testing, Cem. Concr. Res. 42 (2012) 223–243.
[31] B. Lothenbach, F. Winnefeld, C. Alder, E. Wieland, P. Lunk, Effect of temperature on the pore solution, microstructure and hydration products of Portland cement pastes, Cem. Concr. Res. 37 (2007) 483–491.
[32] A. Vollpracht, B. Lothenbach, R. Snellings, J. Haufe, The pore solution of blended cements: a review, Mater. Struct. 49 (2016) 3341–3367.
[33] M. Kasaniya, M.D.A. Thomas, Role of the alkalis of supplementary cementing materials in controlling pore solution chemistry and alkali-silica reaction, Cem. Concr. Res. 162 (2022), 107007.
[34] M. Kasaniya, M.D.A. Thomas, E.G. Moffatt, Efficiency of natural pozzolans, ground glasses and coal bottom ashes in mitigating sulfate attack and alkali-silica reaction, Cem. Concr. Res. 149 (2021), 106551.
[35] B. Meng, P. Fontana, U. Müller, P. Bürgisser, in: H.C. Uzoegbo, W. Schmidt (Eds.), Influence of Natural Pozzolans on the Risk of Alkali Silica Reaction, 2013, pp. 801–808. Johannesburg, South Africa.
[36] Svenska Betongforening, ASR i svensk betong – vägledning för nya och befintliga konstruktioner: Betongrapport nr 18 – Utgåva 1, 2019.
[37] Norwegian Concrete Association (NCA/NB) Committee, NB Publication No. 21: Durable Concrete With Alkali Reactive Aggregate, Oslo, Norway, 2008 (accessed 11 January 2023).
[38] RILEM, AAR-7.1: International Specification to Minimise Damage From Alkali Reactions in Concrete: Part 1: Alkali-Silica Reaction, 2014.
[39] BRE, Alkali-Silica Reaction in Concrete, BRE Bookshop, Watford, England, 2004.
[40] T.F. Rønning, B.J. Wigum, J. Lindgård, Recommendation of RILEM TC 258-AAA: RILEM AAR-10: determination of binder combinations for non-reactive mix design using concrete prisms–38 °C test method, Mater. Struct. 54 (2021) 204.
[41] D. Hooton, M.D.A. Thomas, T. Ramlochan, Use of pore solution analysis in design for concrete durability, Adv. Cem. Res. 22 (2010) 203–210.
[42] P.J. Nixon, C.L. Page, R. Bollinghaus, I. Canham, D.W. Hobbs, M. Ben Haha, The effect of a Pfa with a high total alkali content on pore solution composition and alkali silica reaction, Mag. Concr. Res. 39 (1987) 51–54.
[43] Y. Kawabata, K. Yamada, Evaluation of alkalinity of pore solution based on the phase composition of cement hydrates with supplementary cementitious materials and its relation to suppressing ASR expansion, ACT 13 (2015) 538–553.
[44] M.J. Tapas, L. Sofia, K. Vessalas, P. Thomas, V. Sirivivatnanon, K.L. Scrivener, Efficacy of SCMs to mitigate ASR in systems with higher alkali contents assessed by pore solution method, Cem. Concr. Res. 142 (2021), 106353.
[45] M. Kasaniya, M.D.A. Thomas, Investigating supplementary cementing materials for alkalis and pore fluid properties, in: J.I. Escalante-Garcia, P. Castro Borges, A. Duran-Herrera (Eds.), Proceedings of the 75th RILEM Annual Week 2021, Springer International Publishing, Cham, 2023, pp. 13–21.
[46] P. Rivard, M.A. Bérubé, J.-P. Ollivier, G. Ballivy, Decrease of pore solution alkalinity in concrete tested for alkali-silica reaction, Mater. Struct. 40 (2007) 909–921.
[47] J. Duchesne, M.A. Bérubé, Effect of supplementary cementing materials on the composition of cement hydration products, Adv. Cem. Based Mater. 2 (1995) 43–54.
[48] S. Wei, K. Zheng, J. Zhou, G. Prateek, Q. Yuan, The combined effect of alkalis and aluminum in pore solution on alkali-silica reaction, Cem. Concr. Res. 154 (2022), 106723.
[49] I. Fily-Paré, Behaviour of Concrete Incorporating Ground Glass and Alkali-reactive Aggregates, PhD, 2020.
[50] A. Leemann, B. Lothenbach, The influence of potassium–sodium ratio in cement on concrete expansion due to alkali-aggregate reaction, Cem. Concr. Res. 38 (2008) 1162–1168.
[51] A. Leemann, B. Lothenbach, C. Thalmann, Influence of superplasticizers on pore solution composition and on expansion of concrete due to alkali-silica reaction, Constr. Build. Mater. 25 (2011) 344–350.
[52] F. Deschner, B. Lothenbach, F. Winnefeld, J. Neubauer, Effect of temperature on the hydration of Portland cement blended with siliceous fly ash, Cem. Concr. Res. 52 (2013) 169–181.
[53] P. Rivard, M.A. Bérubé, J.-P. Ollivier, G. Ballivy, Alkali mass balance during the accelerated concrete prism test for alkali–aggregate reactivity, Cem. Concr. Res. 33 (2003) 1147–1153.
[54] H.F.W. Taylor, A method for predicting alkali ion concentrations in cement pore solutions, Adv. Cem. Res. 1 (1987) 5–17.
[55] C. Balachandran, J.F. Muñoz, S. Peethamparan, T.S. Arnold, Alkali -silica reaction and its dynamic relationship with cement pore solution in highly reactive systems, Constr. Build. Mater. 362 (2023), 129702.
[56] K. De Weerdt, M. Ben Haha, G. Le Saout, K.O. Kjellsen, H. Justnes, B. Lothenbach, Hydration mechanisms of ternary Portland cements containing limestone powder and fly ash, Cem. Concr. Res. 41 (2011) 279–291.
[57] B. Traynor, H. Uvegi, E. Olivetti, B. Lothenbach, R.J. Myers, Methodology for pH measurement in high alkali cementitious systems, Cem. Concr. Res. 135 (2020), 106122.
[58] K.L. Scrivener, R. Snellings, B. Lothenbach (Eds.), A Pratical Guide to Microstructural Analysis of Cementitious Materials, CRC Taylor & Francis, Boca Raton, 2017.
[59] D. Jansen, F. Goetz-Neunhoeffer, C. Stabler, J. Neubauer, A remastered external standard method applied to the quantification of early OPC hydration, Cem. Concr. Res. 41 (2011) 602–608.
[60] W.G. Mumme, R.J. Hill, G. Bushnellwye, E.R. Segnit, Rietveld crystal-structure refinements, crystal-chemistry and calculated powder diffraction data for the polymorphs of dicalcium silicate and related phases, N. Jahrb. Mineral. Abh. 169 (1995) 35–68.
[61] K.L. Scrivener, A. Bazzoni, B. Mota, J.E. Rossen, Electron microscopy, in: K. L. Scrivener, R. Snellings, B. Lothenbach (Eds.), A Pratical Guide to Microstructural Analysis of Cementitious Materials, CRC Taylor & Francis, Boca Raton, 2017.
[62] P. Zuschlag, The Impact of Curing Temperatures on Portland Composite Cements - Hydrate Assemblage, Porosity, and Compressive Strength, PhD thesis, Trondheim, Norway, 2022.
[63] P.T. Durdziński, C.F. Dunant, M.B. Haha, K.L. Scrivener, A new quantification method based on SEM-EDS to assess fly ash composition and study the reaction of its individual components in hydrating cement paste, Cem. Concr. Res. 73 (2015) 111–122.
[64] K.L. Aughenbaugh, R.T. Chancey, P. Stutzman, M.C. Juenger, D.W. Fowler, An examination of the reactivity of fly ash in cementitious pore solutions, Mater. Struct. 46 (2013) 869–880.
[65] Norwegian Concrete Association (NCA/NB) Committee, NB Publication No. 32: Alkali-Silica Reaction in Concrete. Test Methods and Requirements to Laboratories, Oslo, Norway, 2005 (accessed 11 January 2023).
[66] I. Borchers, J. Lindgård, T.F. Rønning, B.J. Wigum, Recommendation of RILEM TC 258-AAA: RILEM AAR-11: determination of binder combinations for non-reactive mix design or the resistance to alkali-silica reaction of concrete mixes using concrete prisms – 60 °C test method, Mater. Struct. 54 (2021) 203.
[67] E. Gallucci, X. Zhang, K.L. Scrivener, Effect of temperature on the microstructure of calcium silicate hydrate (C-S-H), Cem. Concr. Res. 53 (2013) 185–195.
[68] K. De Weerdt, M. Ben Haha, G. Le Saout, K.O. Kjellsen, H. Justnes, B. Lothenbach, The effect of temperature on the hydration of composite cements containing limestone powder and fly ash, Mater. Struct. 45 (2012) 1101–1114.
[69] K.O. Kjellsen, R.J. Detwiler, O.E. Gjørv, Development of microstructures in plain cement pastes hydrated at different temperatures, Cem. Concr. Res. 21 (1991) 179–189.
[70] R. Snellings, A. Machner, G. Bolte, H. Kamyab, P.T. Durdziński, P. Teck, M. Zajac, A.C.A. Muller, K. De Weerdt, M.B. Haha, Hydration kinetics of ternary slag-limestone cements: impact of water to binder ratio and curing temperature, Cem. Concr. Res. 151 (2022), 106647.
[71] R.J. Myers, E. L'Hôpital, J.L. Provis, B. Lothenbach, Effect of temperature and aluminium on calcium (alumino)silicate hydrate chemistry under equilibrium conditions, Cem. Concr. Res. 68 (2015) 83–93.
[72] I.G. Richardson, Model structures for C-(A)-S-H(I), Acta Crystallogr. Sect. B: Struct. Sci. Cryst. Eng. Mater. 70 (2014) 903–923.
[73] M.B. Haha, B. Lothenbach, G. Le Saout, F. Winnefeld, Influence of slag chemistry on the hydration of alkali-activated blast-furnace slag — part II: effect of Al2O3, Cem. Concr. Res. 42 (2012) 74–83.
[74] P. Hemstad, A. Machner, K. De Weerdt, The effect of artificial leaching with HCl on chloride binding in ordinary Portland cement paste, Cem. Concr. Res. 130 (2020), 105976.
[75] Z. Shi, S. Park, B. Lothenbach, A. Leemann, Formation of shlykovite and ASR-P1 in concrete under accelerated alkali-silica reaction at 60 and 80 °C, Cem. Concr. Res. 137 (2020), 106213.
[76] X. Zhang, Quantitative Microstructural Characterisation of Concrete Cured Under Realistic Temperature Conditions, PhD, Leusanne, Switzerland, 2007.
[77] S. Bahafid, S. Ghabezloo, M. Duc, P. Faure, J. Sulem, Effect of the hydration temperature on the microstructure of Class G cement: C-S-H composition and density, Cem. Concr. Res. 95 (2017) 270–281.
[78] F. Avet, K.L. Scrivener, Effect of temperature on the water content of C-A-S-H in plain Portland and blended cements, Cem. Concr. Res. 136 (2020), 106124.
[79] W. Chen, H.J.H. Brouwers, Alkali binding in hydrated Portland cement paste, Cem. Concr. Res. 40 (2010) 716–722.
[80] T.T.H. Bach, E. Chabas, I. Pochard, C. Cau Dit Coumes, J. Haas, F. Frizon, A. Nonat, Retention of alkali ions by hydrated low-pH cements: mechanism and Na+/K+ selectivity, Cem. Concr. Res. 51 (2013) 14–21.

[81] Y. Kawabata, K. Yamada, G. Igarashi, Y. Sagawa, Effects of soak solution type on alkali release from volcanic aggregates – is alkali release really responsible for accelerating ASR expansion? ACT 16 (2018) 61–74.
[82] Z. Shi, B. Lothenbach, The combined effect of potassium, sodium and calcium on the formation of alkali-silica reaction products, Cem. Concr. Res. 127 (2020), 105914.
[83] G. Plusquellec, M.R. Geiker, J. Lindgård, J. Duchesne, B. Fournier, K. De Weerdt, Determination of the pH and the free alkali metal content in the pore solution of concrete: review and experimental comparison, Cem. Concr. Res. 96 (2017) 13–26.
[84] F. Georget, W. Wilson, K.L. Scrivener, edxia: microstructure characterisation from quantified SEM-EDS hypermaps, Cem. Concr. Res. 141 (2021), 106327.
[85] B. Münch, L.H.J. Martin, A. Leemann, Segmentation of elemental EDS maps by means of multiple clustering combined with phase identification, J. Microsc. 260 (2015) 411–426.
[86] T. Matschei, B. Lothenbach, F.P. Glasser, The AFm phase in Portland cement, Cem. Concr. Res. 37 (2007) 118–130.
[87] F. Georget, B. Lothenbach, W. Wilson, F. Zunino, K.L. Scrivener, Stability of hemicarbonate under cement paste-like conditions, Cem. Concr. Res. 153 (2022), 106692.